

Alkaline magmas in zones of continental convergence: The Tezhsar volcano-intrusive ring complex, Armenia



Krzysztof Sokół ^{a,1}, Ralf Halama ^{a,*}, Khachatur Meliksetian ^b, Ivan P. Savov ^c, Gevorg Navasardyan ^b, Masafumi Sudo ^d

^a School of Geography, Geology and the Environment, Keele University, Keele ST5 5BG, United Kingdom

^b Institute of Geological Sciences, Armenian National Academy of Sciences, 24a Marshal Baghramian Avenue, 0019 Yerevan, Armenia

^c School of Earth and Environment, University of Leeds, Leeds LS2 9JT, United Kingdom

^d Institute of Earth and Environmental Science, University of Potsdam, Karl-Liebknecht-Str. 24-25, 14476 Potsdam, Germany

ARTICLE INFO

Article history:

Received 5 April 2018

Accepted 24 August 2018

Available online 31 August 2018

Keywords:

Alkaline igneous rocks

Ring complex

Armenia

Geochemistry

⁴⁰Ar/³⁹Ar dating

Pseudoleucite

ABSTRACT

Alkaline igneous rocks are relatively rare in settings of tectonic convergence and little is known about their petrogenesis in these settings. This study aims to contribute to a better understanding of the formation of alkaline igneous rocks by an investigation of the Tezhsar volcano-intrusive alkaline ring complex (TAC) in the Armenian Lesser Caucasus, which is located between the converging Eurasian and Arabian plates. We present new petrological, geochemical and Sr–Nd isotope data for the TAC to constrain magma genesis and magma source characteristics. Moreover, we provide a new ⁴⁰Ar/³⁹Ar age of 41.0 ± 0.5 Ma on amphibole from a nepheline syenite that is integrated into the regional context of ongoing regional convergence and widespread magmatism. The TAC is spatially concentric and measures ~10 km in diameter representing the relatively shallow plumbing system of a major stratovolcano juxtaposed by ring faulting with its extrusive products. The plutonic units comprise syenites and nepheline syenites, whereas the extrusive units are dominated by trachytic-phonolitic rocks. The characteristic feature of the TAC is the development of pseudomorphs after leucite in all types of the volcanic, subvolcanic and intrusive alkaline rocks.

Whole-rock major element data show a metaluminous (Alkalinity Index = 0–0.1), alkalic and silica-undersaturated (Feldspathoid Silica-Saturation Index <0) character of the TAC. The general trace element enrichment and strong fractionation of REEs (La_N/Yb_N up to 70) indicate a relatively enriched magma source and small degrees of partial melting. All TAC rocks show a negative Nb–Ta anomalies typical of subduction zone settings. The initial ⁸⁷Sr/⁸⁶Sr ratios (0.704–0.705) and positive εNd values (+3 to +5) indicate an isotopically depleted upper mantle and lack of significant crustal influence, which in turn suggests the TAC magma has formed via differentiation from lithospheric mantle melts.

Regionally, the age of ~41 Ma places the TAC amid a Lesser Caucasian Eocene period of dominantly calc-alkaline magmatism. The TAC's arc-like geochemical signatures are interpreted to result from prior subduction of the Tezhsar slab beneath the Eurasian continental margin. The alkaline character, distinct from regional trends, is attributed to Neotethyan slab rollback causing extension and inducing small degrees of decompression melting of metasomatised lithospheric mantle.

© 2018 Elsevier B.V. All rights reserved.

1. Introduction

Studies of alkaline magmatism on the global scale have become a point of focus due to the significant role of alkaline magmatic rocks for ore exploration, in particular regarding prospecting for rare earth

elements (REEs), niobium (Nb), tantalum (Ta) and zirconium (Zr) (e.g. Chakhmouradian & Zaitsev, 2012). Many alkaline igneous rocks are found in rift-related intraplate settings (e.g. Gardar Province/Greenland, Upton et al., 2003; Kola Alkaline Province/Russia, Downes et al., 2005; East African Rift, Woolley, 2001), but they also occur, albeit less frequently, in settings of plate convergence (Burke & Khan, 2006; Hou et al., 2006). Plate convergence includes collisional events that cause the welding of terranes into continental land and subsequent post-collisional episodes in which convergence continues (Bonin et al., 1998). The occurrence of magmas with alkaline affinities becomes more common only when the geodynamic context becomes entirely intraplate

* Corresponding author.

E-mail address: r.halama@keele.ac.uk (R. Halama).

¹ Present address: School of Earth and Environmental Sciences, University of St Andrews, St Andrews, KY16 9AL, United Kingdom.

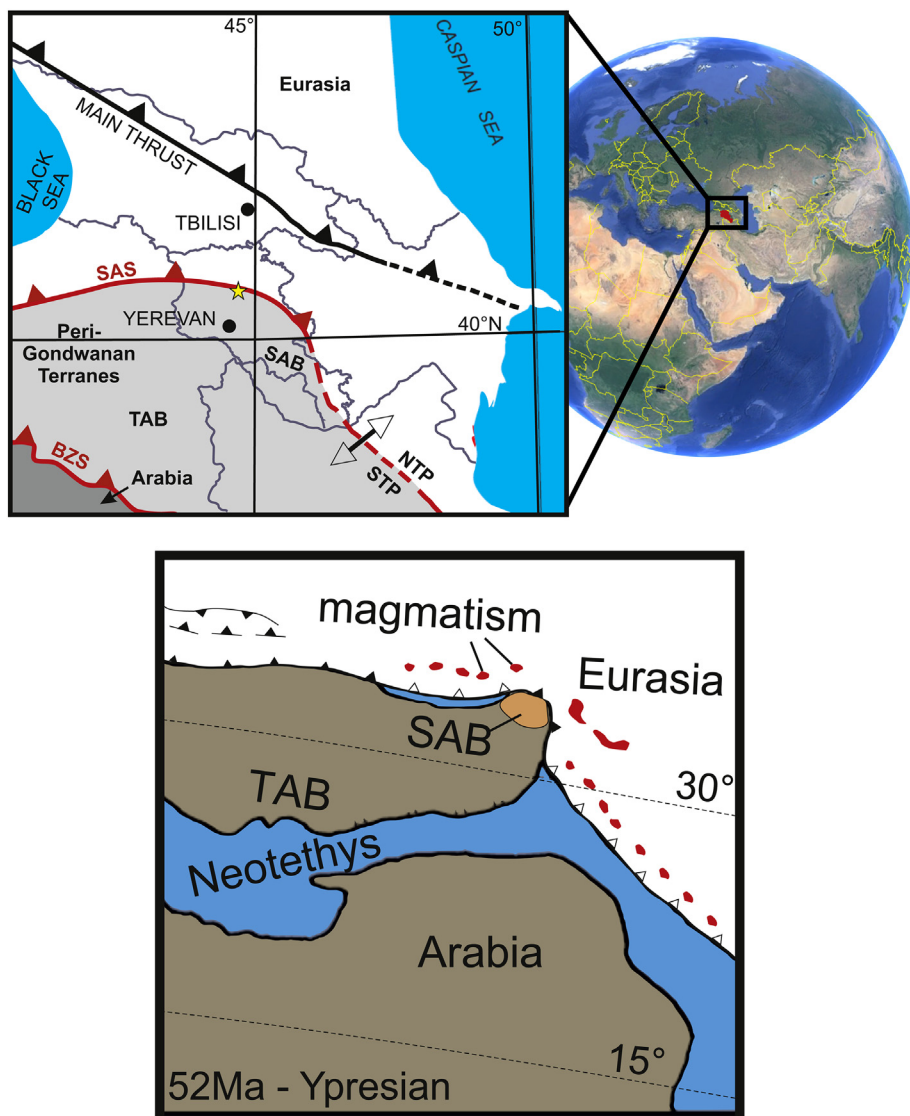


Fig. 1. (a) Geotectonic framework of the Caucasus region showing major tectonostratigraphic provinces, associated terranes and the location of Tezhsar Alkaline Complex (star) about 50 km north of Yerevan (modified after Adamia et al., 2011, and Rezeau et al., 2017). (b) Palaeogeographical reconstruction of the Eurasian-Arabian collision in the Ypresian (52 Ma) just before formation of TAC (modified after Mederer et al., 2013). SAB – South Armenian Block, SAS – Sevan-Akera Suture, BZS – Bitlis-Zagros Suture, TAB – Tauride-Anatolian Block, NTP – Northern Tethyan Province, STP – Southern Tethyan Province.

in a post-orogenic episode (Bonin et al., 1998). In complex collisional and post-collisional settings, the timing of specific types of magmatism depends on the geotectonic geometries and the relative rates of crustal thickening and subsidiary subduction (Harris et al., 1986). Importantly, convergent movement between colliding plates will continue for 30–50 Ma after the initial collision (Harris et al., 1986). On a global scale, deformed alkaline rocks and carbonatites (DARCs) may be used as indicators of where ancient oceans have opened and closed, and the presence of a variety of syenites, carbonatites and other alkaline igneous rocks found in proximity to older DARCs indicate the recycling of material from the underlying lithosphere based on the Wilson Cycle-type model (Burke & Khan, 2006). Thus, investigating alkaline magmatism in convergent settings, e.g. in Tibet (Hou et al., 2006; Williams et al., 2004) and the Anatolian-Armenian-Iranian plateau (Jackson et al., 1995; Neill et al., 2015), has become as important as studies of rift-related settings to understand alkaline magma genesis.

The exact mechanisms responsible for magma generation in collisional tectonic settings remain enigmatic. Models include slab break-off (Keskin, 2003; Neill et al., 2015; Van Hunen & Allen, 2011), large-scale delamination or thinning of the lithospheric mantle (Innocenti et

al., 1982; Pearce et al., 1990) and small-scale lithospheric detachment driven by convection cells (Kaislaniemi et al., 2014; Neill et al., 2015). Moreover, the source of magmas in compressional regimes and their chemical impact on the crust remains disputed. Processes to generate primary magmas in collision zones may involve melting of thickened lithosphere due to breakdown of hydrous phases at the continental suture (Allen et al., 2013) and melting of deeply-subducted continental crust (Zhao et al., 2013). To explain the alkaline character of the erupted or plutonic igneous rocks, several genetic models and processes have been proposed:

1. Low degrees of partial melting of metasomatized upper mantle (Bodevign et al., 2017; Dawson, 1987; Marks et al., 2008).
2. Melting of crustal sources, which could be located in the lower crust and mafic in composition (Smith et al., 1988) or in the middle to upper crust and felsic in composition (Downes, 1987; Fitton, 1987).
3. Fractional crystallization from alkali basalt parental magmas (Delong et al., 1975; Trumbull et al., 2003), with variable degrees of crustal assimilation (Fitton, 1987; Jung et al. 2007; Lan et al., 2011).

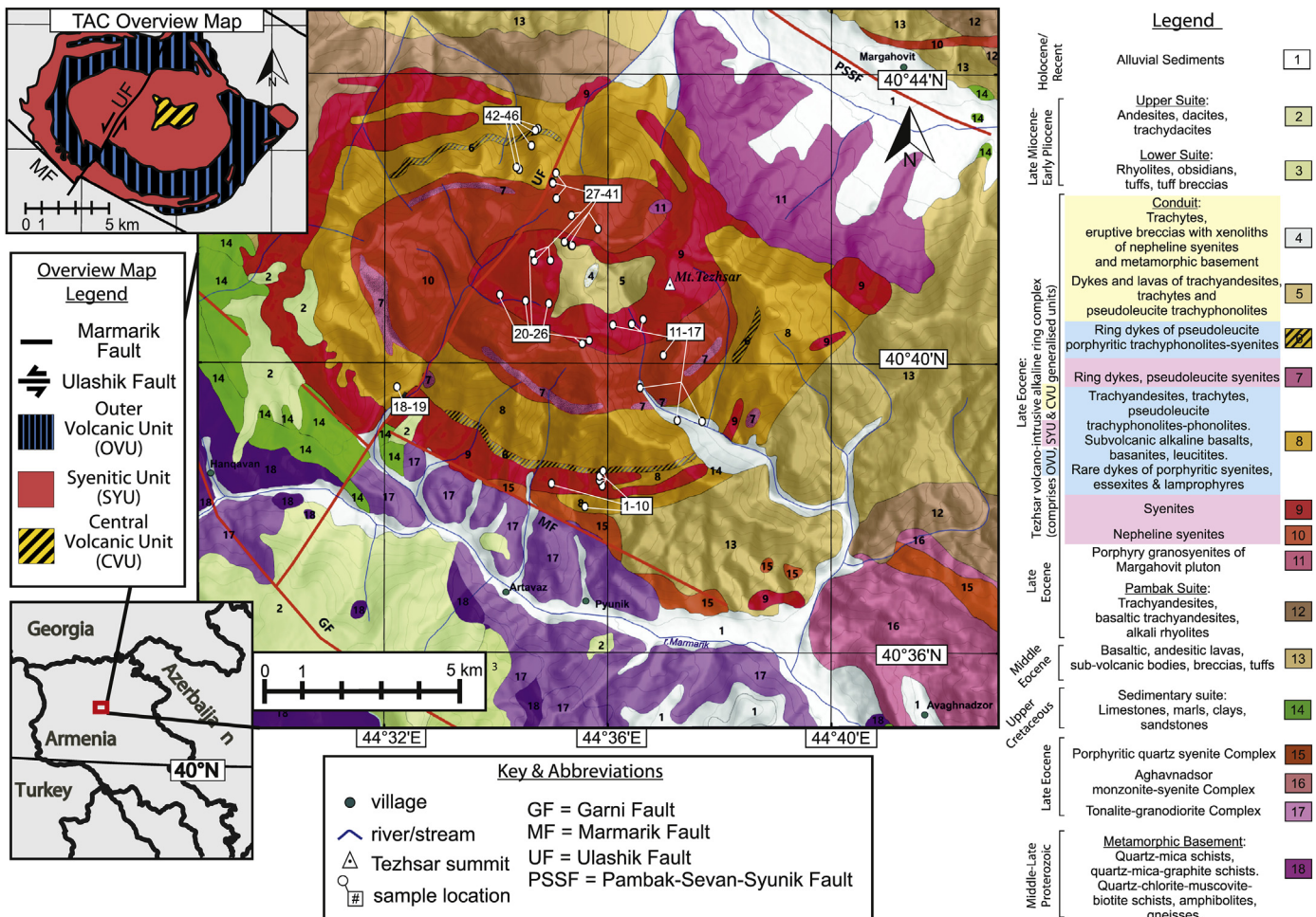


Fig. 2. Geological map of the Tezhzar Alkaline Complex. The map is based on earlier geological maps produced by G. Baghdasaryan and B. Meliksetian. The inset show a simplified subdivision of the TAC which is used for the geochemical diagrams of this study.

4. Fenitisation – a high temperature metasomatic alteration driven by alkali-rich fluids incrementally expelled from alkaline or carbonatitic melts (Sindern & Kramm, 2000; Suikkanen & Rämö, 2017).

Armenia, landlocked between the Black Sea and the Caspian Sea, forms part of the Anatolian-Armenian-Iranian Plateau and is characterized by widespread Cenozoic volcano-magmatic activity, starting in the Eocene at ~50 Ma and intermittently lasting into the Holocene and historical times (Karakhanian et al., 2002; Moritz et al., 2016; Fig. 1a). Several studies focused on Quaternary volcanic cones on the Anatolian-Armenian-Iranian plateau (Innocenti et al., 1982; Keskin et al., 1998; Pearce et al., 1990), including in the Armenian segments of the Lesser Caucasus mountain range (Karakhanian et al., 2002; Karapetian et al., 2001), and the Miocene/Pliocene magmatic evolution of the region (Dilek et al., 2010; Kheirkhah et al., 2015; Neill et al., 2013). However, investigating the much less studied Paleogene igneous rocks is important to gain a more complete understanding of the long-term magmatic and geodynamic evolution in this setting of continuing convergence and to improve our understanding of collision-driven continental magmatism and mantle dynamics (Dilek et al., 2010; Moritz et al., 2016; Van Hunen & Allen, 2011).

In this study, we use a range of petrological and geochemical methods to describe and interpret the lithological variations of the Tezhzar volcano-intrusive alkaline ring complex (or Tezhzar Alkaline Complex - TAC) in Armenia. We provide a new $^{40}\text{Ar}/^{39}\text{Ar}$ age and expand on previous petrological and geochemical studies (Kogarko et al.

1995; Magakyan 1981; Meliksetian, 1971, 1989) with the aim to achieve a better understanding of TAC petrogenesis and to integrate that into a model of alkaline magma genesis within a setting of continuing plate convergence. We also highlight and discuss the occurrence of cm-sized pseudoleucites in the TAC.

2. Geological history

2.1. Regional tectonic setting

The TAC, located about 55 km north of Yerevan in the Lesser Caucasus, has formed in the Eocene in a setting of general convergence between the Eurasian and Arabian plates (Fig. 1a). This region was affected by two distinct collisional events and the emplacement of the alkaline magmas of the TAC is crucial to the understanding of the tectono-magmatic evolution of the region.

The TAC is located on basement of the South Armenian Block (SAB), which is a microplate of Gondwanaland origin (Knipper & Khain, 1980; Rolland, 2017; Sosson et al., 2010). Proterozoic metamorphic basement of the SAB is exposed in the Tsakhkunyats massif (Aghamalyan, 1998; Belov, 1968). Platform sedimentary cover of the SAB is presented by folded Late Devonian to the Late Triassic sedimentary formations (Arakelyan, 1964; Aslanyan, 1958). Ophiolites representing Jurassic oceanic crust were obducted onto the northern margin of the SAB in the Late Cretaceous (90–84 Ma; Rolland, 2017). In the late Cretaceous to early Palaeogene (70–60 Ma), the SAB was welded to the southern

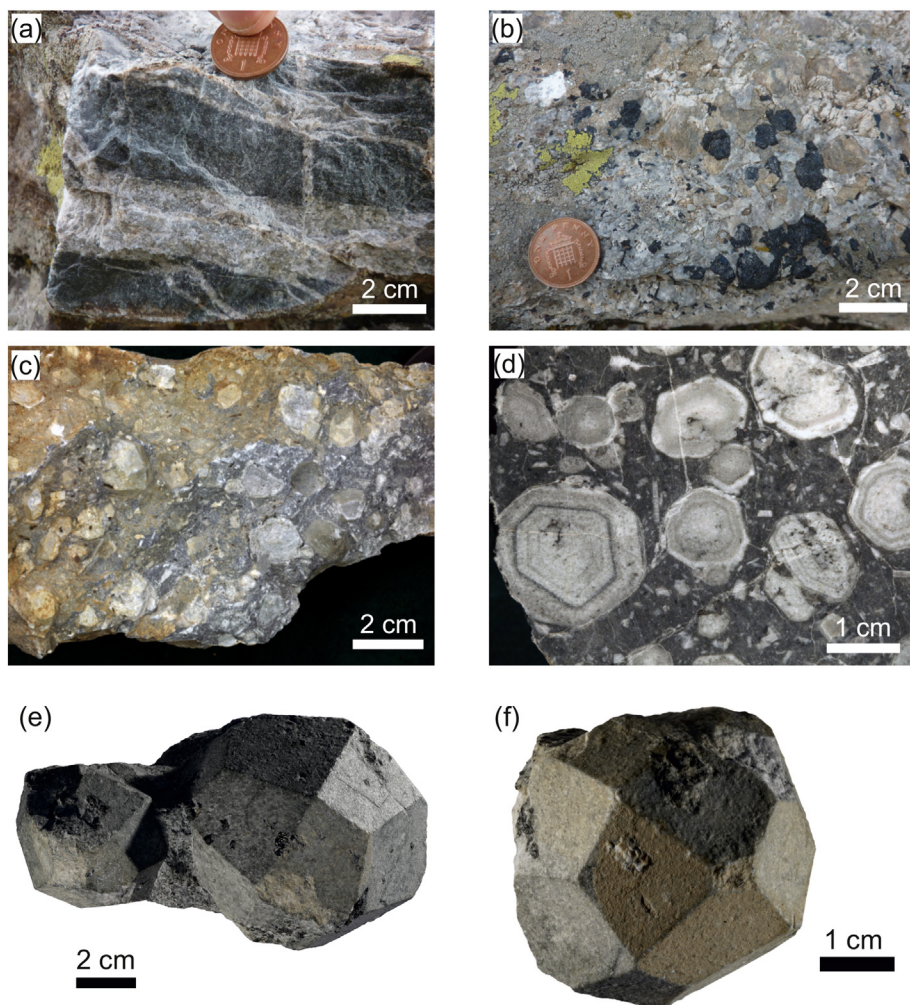


Fig. 3. Field relations (a, b) and hand specimen photographs (c, d) of the TAC. (a) Light coloured syenite intruding into dark grey volcanic rocks of the Outer Volcanic Unit. (b) Coarse-grained nepheline syenite pegmatite comprising dark patches of garnet and amphibole. (c) Phonolite hand specimen with idiomorphic leucite pseudomorphs reaching up to 2 cm in diameter. (d) Polished surface of a pseudoleucite phonolite. (e, f) Hand specimen of pseudoleucite megacrysts (up to ~8 cm in diameter) as deltoidal icositetrahedra found in TAC phonolites. Samples are from old collections of B. Meliksetian and Z. Chibukhyan.

margin of Eurasia as a result of the closure of the northern branch of the Neotethys and the termination of subduction (Moritz et al., 2016; Rolland et al., 2009b; Rolland et al., 2009a). The collision is marked by the Sevan-Akera suture zone, which is part of the regional northern Neotethys suture (Hässig et al., 2013; Sosson et al., 2010). The closure of the northern Neotethys branch caused a subduction jump towards the south and the accretion of the SAB to the Eurasian margin resulted in formation of a Cretaceous-Eocene flysch basin that overlies the ophiolites (Rolland, 2017). At present, the Sevan-Akera suture separates two tectonostratigraphic units, the Southern and Northern Tethyan Provinces, which outline the continental provinces pre-dating the closure of the Tethys Ocean (Fig. 1b; Adamia et al., 2011). The Sevan-Akera suture is located ~6 km northward of the TAC. The second stage of accretion involving collision of the Arabian margin to the SAB and the Tauride-Anatolian block caused the closure of the South Neotethys ocean along the Bitlis-Zagros suture. This closure occurred in late Eocene to early Oligocene times (40–25 Ma) based on geochronological and structural evidence (Agard et al., 2005; Allen & Armstrong, 2008; Rolland, 2017). The convergence and collision between Arabia and Eurasia induced regional compression and shortening in the overriding (SAB-Eurasia) continental lithosphere (Agard et al., 2011), the formation of the Anatolian-Armenian-Iranian orogenic plateau (Sheth et al.,

2015) and lateral ejection of the Anatolian and Iranian blocks, with the Armenian Highland (Lesser Caucasus and Eastern Anatolia) in the centre (Phillip et al., 1989). Protracted Cenozoic magmatism lasted from ~49 Ma to ~21 Ma and marked the final stages of the Neothethyan subduction, the main Arabia-Eurasia collisions and subsequent post-collisional events, including emplacement of the syn-collisional granite-leucogranite plutons of the Lesser Caucasus (Meliksetian, 1989; Rezeau et al., 2017).

To explain the Palaeogene magmatism of the entire region, Dilek et al. (2010) proposed the opening of an asthenospheric window beneath the arc mantle wedge and the collision zone. The presence of adakites of Early Eocene age in the Pontides interpreted as a result of slab window formation (Eyuboglu et al., 2011) supports this hypothesis. Lordkipanidze et al. (1989) and Sahakyan et al. (2016) consider a subduction-modified upper mantle source for Lower-Middle Eocene volcanism and an increase of crustal input within the Late Eocene-Early Oligocene magmatic series of the Lesser Caucasus.

Considering the age and location of the TAC ($^{40}\text{Ar}/^{39}\text{Ar}$ of 41.0 ± 0.5 Ma, this study; 36.3–37.5 Ma, K—Ar, Bagdasaryan et al., 1985; 36–39 Ma, K—Ar, Meliksetian, 1989), it formed in a plate convergence setting, in between two major collisional events that occurred in region – first at the northern edge of the SAB in the Late Cretaceous to Early Paleogene,

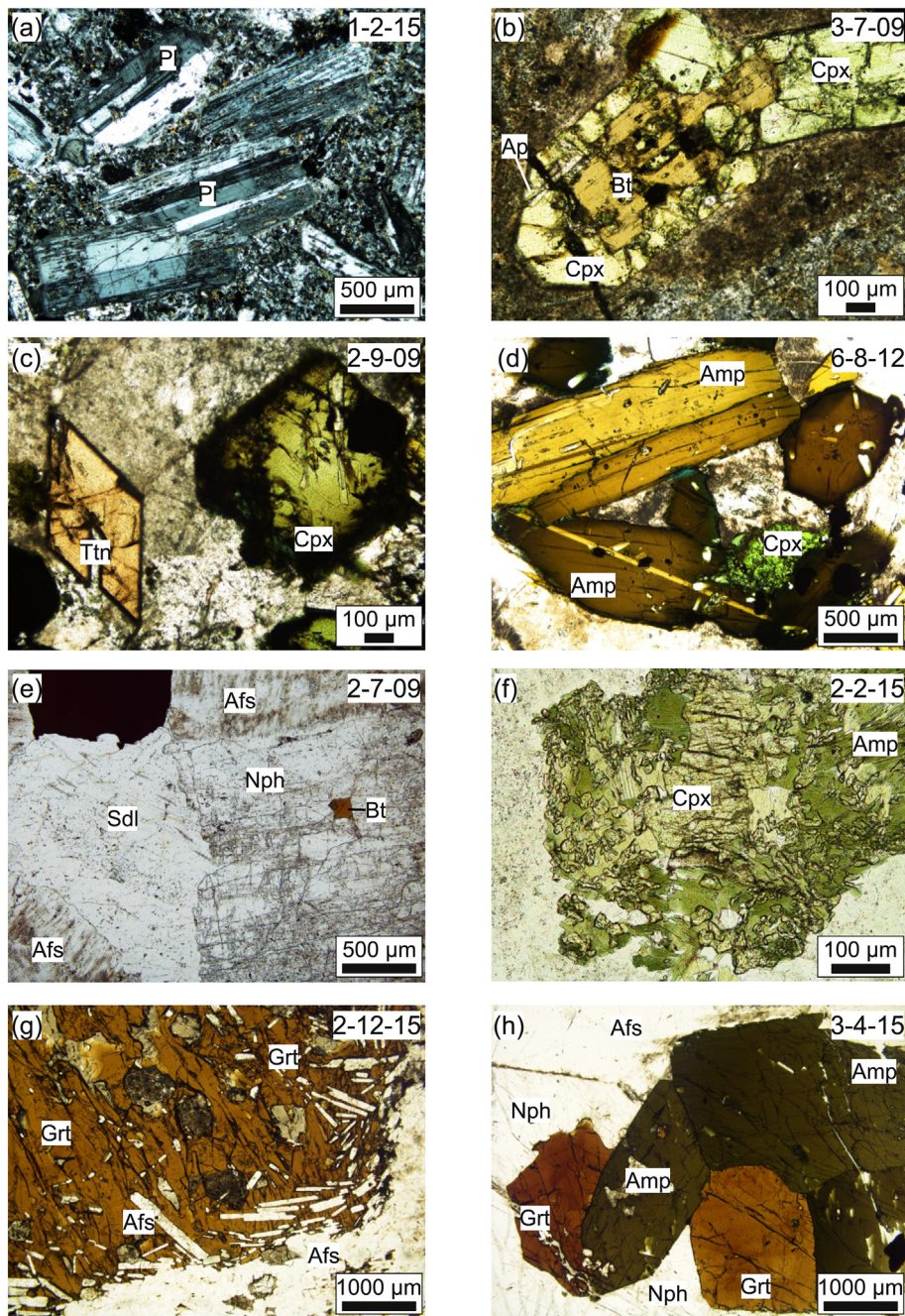


Fig. 4. Photomicrographs illustrating characteristic features of rocks from the TAC in plane polarized (PPL) and cross-polarized (XPL) light. (a) Plagioclase (Pl) phenocrysts in feldspathic matrix of a basaltic trachyandesite, OVU (XPL). (b) Biotite (Bt) surrounded by clinopyroxene (Cpx) with accessory apatite (Ap) in trachyte, CVU (PPL). (c) Clinopyroxene and titanite (Ttn) in nepheline syenite, SYU (PPL). (d) Amphibole (Amp) in syenite, SYU (PPL). (e) Sodalite (Sdl) and nepheline (Nph) in nepheline syenite, SYU (PPL). (f) Amphibolitization of clinopyroxene in syenite, SYU (PPL). (g) Garnet (Grt) in syenite with inclusions of alkali feldspar, SYU (PPL). (h) Garnet-amphibole cluster with alkali feldspar and nepheline in pegmatitic nepheline syenite, SYU (PPL).

and subsequently to the south of the SAB in the Late Eocene to Early Oligocene. The TAC can thus be described as post-collisional relative to the initial collisional event between the SAB and the Eurasian plate.

2.2. Geological setting of the Tezhser Alkaline complex

The TAC is located on the Pambak ridge at the northern edge of the SAB within the Sevan-Shirak basin. To the south, the TAC is in contact with the Proterozoic metamorphic basement of the SAB across the Marmarik Fault. Presence of abundant xenoliths from the Tsakhkunyats basement, such as mica schists, confirms the affinity of the TAC to the SAB continental terrane. To the north, the TAC borders the Margahovit

intrusion comprising porphyritic granosyenites. Country rocks exposed to the W-NW of the TAC comprise Upper Cretaceous clastic and carbonate strata and Mid-to-Late Eocene extrusive igneous rocks, which also outcrop to the E-SE. The Ulashik Fault cuts the TAC in SW-NE direction with horizontal left-lateral displacement of intrusive and volcanic units reaching 700 m.

The TAC represents a ring complex that can be subdivided into several concentric units of both volcanic and plutonic rocks. Such classical ring complexes are quite rare (Johnson et al., 1999) and are of special interest considering their structural and volcanological evolution as well as petrological aspects. According to Meliksetian (1971), the TAC includes the following major units (Fig. 2):

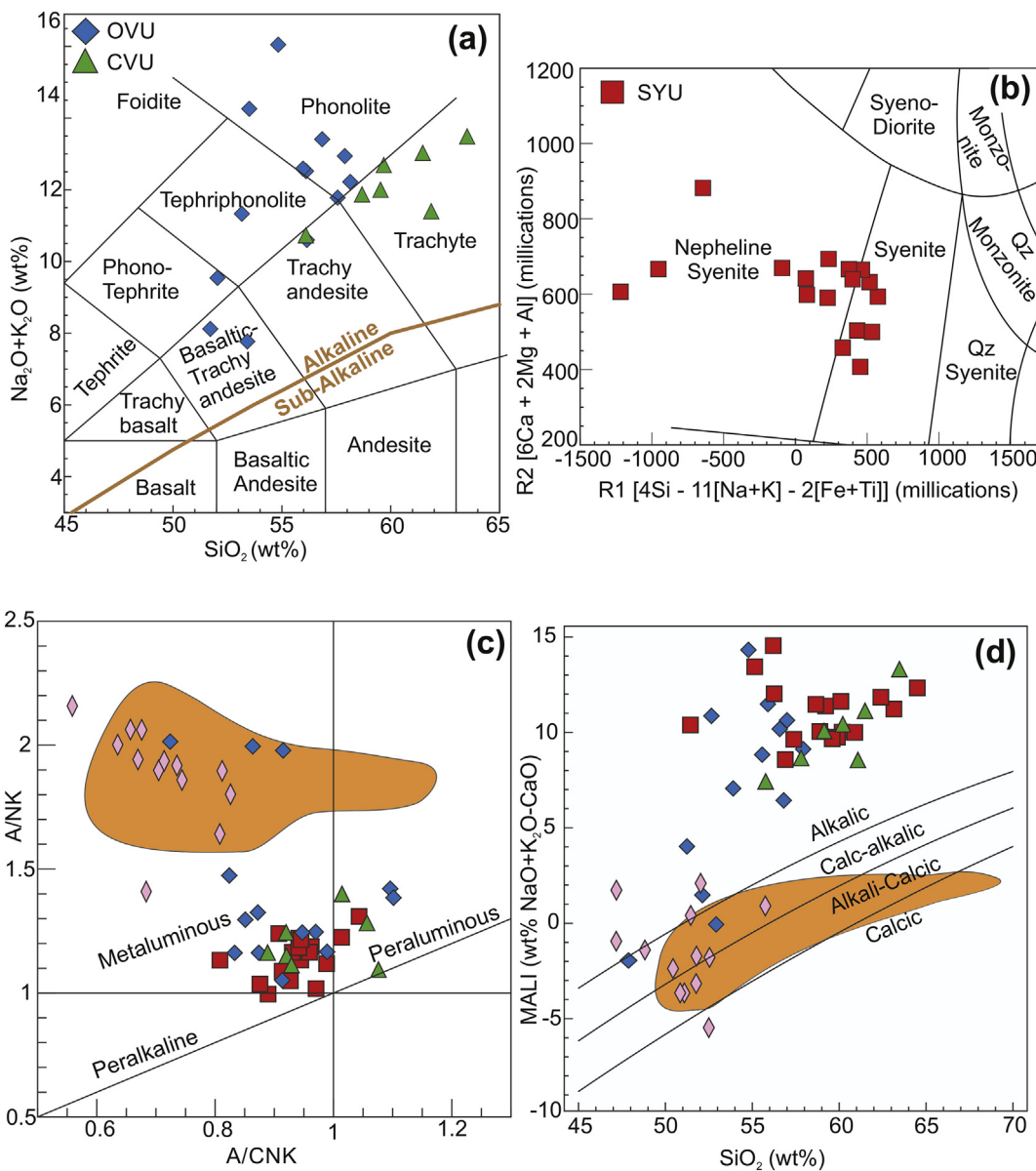


Fig. 5. (a) Total Alkali-Silica (TAS) classification diagram of the volcanic units (OVU and CVU) of the TAC. Alkaline-subalkaline division from Irvine and Baragar (1971). (b) R1-R2 classification diagram (from De La Roche et al., 1980) of the intrusive SYU unit of the TAC. (c) A/NK vs A/CNK diagram (after Shand, 1947) based on the molecular proportions of Al (A), Na (N), K (K) and Ca (C), showing that the rocks of the TAC can largely be classified as metaluminous. (d) Modified Alkali-Lime Index (MALI, after Frost & Frost, 2008) plotted as a function of SiO_2 content for the TAC rocks that are generally alkalic in composition. Comparative data for Eocene magmatic rocks from the Talysh mountains, Azerbaijan (Vincent et al., 2005 – pink diamonds) and Pliocene-Quaternary volcanic rocks from central and northern Armenia (Neill et al., 2013, 2015 – orange field).

- Outer cone sheets characterized by inward-dipping contacts
- Ring unit of volcanic alkaline rocks with a thickness up to 600 m characterized by its concentric structure and inward-dipping contacts (Outer Volcanic Unit, OUV)
- Central intrusive unit comprising syenites and nepheline syenites (Syenitic Unit, SYU)
- Ring dykes, circular bodies with sub-vertical contacts cutting both the volcanic and central intrusive units
- Resurgent volcanic unit, inside the central intrusive unit, formed by volcanic breccias, dykes and subvolcanic rocks (Central Volcanic Unit, CVU).

For the purpose of the geochemical investigation in this study, we use a simplified subdivision into Outer Volcanic Unit, Syenitic Unit and

Central Volcanic Unit (Fig. 2). Based on a structural analysis including bedding attitudes of units and relationships between volcanic ring, cone sheets and central pluton, the presence of circular dykes and remains of a volcanic centre, most researchers, namely Kotlyar (1958), Bagdasaryan (1966) and Meliksetian (1971) concluded that the TAC formed via a caldera collapse and the volcanic ring was emplaced through collapse along concentric faults. The exceptionally large elliptical palaeocaldera structure of the TAC is $\sim 13.6 \times 11.5$ km in size and has an area of $\sim 131 \text{ km}^2$, comparable in dimensions to the Santorini caldera in the Aegean Sea. Such a ring morphology provides a unique insight into the roots of an alkaline volcano-plutonic complex.

Beyond the petrogenetic and structural significance of the TAC, there is also a characteristic widespread development of pseudomorphs after leucite, which have been studied in detail by Meliksetian (1970, 1971,

1978, 1989) and Yagi and Gupta (1978). They feature in volcanic, subvolcanic and intrusive alkaline rocks and the largest crystals, reaching up to 8 cm in size (Fig. 3) are found in porphyry tinguaita dykes (Meliksetian, 1978; Yagi & Gupta, 1978). Their crystallographic habit is either icositetrahedral (in volcanic rocks and dykes) or triakis octahedral (in intrusive syenites). In the Soviet petrological literature according to Zavaricky (1934), pseudomorphism after leucite is divided into two mineralogical and genetic types: "Pseudoleucites" referring to leucite breakdown into nepheline and orthoclase, and "epileucites" describing pseudomorphism after leucite composed of agglomerated orthoclase, muscovite, analcime, chlorite, calcite and zeolites. In the Western petrological literature, usually both types are referred to as pseudoleucites, and both types have been described in the TAC.

3. Field observations

Field campaigns in the TAC were carried out in 2008, 2012 and 2015 in order to achieve two major aims: i) Help the completion of geological map (incl. GIS database) of the complex; ii) sampling the various lithologies of the TAC for petrological and geochemical investigations (Fig. 2). Sampling was focused on the three major units generalised for the purposes of this study: The Outer Volcanic Unit (OVU), the inner Syenitic Unit (SYU) and the Central Volcanic Unit (CVU) (Fig. 2), which have been juxtaposed by ring faulting. In total, 46 samples were collected and analysed, and one of those (sample 6–8–12 from the SYU) was used for $^{40}\text{Ar}/^{39}\text{Ar}$ age determination. Field relations demonstrate that the syenitic magmas of the SYU intruded into the OUV (Fig. 3a). More localized and subordinate lithologies of the complex include syenitic pegmatites (Fig. 3b) and pseudoleucite-bearing phonolites (Fig. 3c–f).

4. Petrography

The pioneering works of Meliksetian (1989) identified >50 different mineral species in rocks of the TAC, including a variety of rare earth element (REE) and high field strength element (HFSE) bearing phases. In our study, we focus on the major rock-forming minerals in the three major rock units of the complex to provide a general overview of the lithologies.

The volcanic rocks of the Outer Volcanic Unit (OVU) are typically porphyritic with an aphanitic groundmass. Major minerals are plagioclase + clinopyroxene + amphibole + biotite + alkali feldspar + Fe–Ti oxides ± nepheline, and apatite and titanite are present as accessory phases. Plagioclase is euhedral to subhedral, weakly zoned and often shows sieve textures (Fig. 4a). Euhedral clinopyroxene phenocrysts are up to 2 mm in size and typically poikilitic. Volcanic breccias are observed occasionally, containing angular fragments and xenoliths, the latter partly rich in quartz. Volumetrically small occurrences of altered pseudoleucite phonolites are present, where we found pseudomorphed leucite up to several cm in diameter. The deltoidal icositetrahedral crystal habit of the primary leucite is well preserved, but leucite has been completely replaced by secondary minerals. These are dominated by alkali feldspar and cancrinite-group minerals and comprise minor amounts of analcime. Other phases found in the pseudoleucite are clinopyroxene, biotite, apatite and calcite.

The volcanic rocks of the Central Volcanic Unit (CVU) are generally porphyritic with a fine-grained matrix. They contain euhedral plagioclase + alkali feldspar + clinopyroxene + amphibole + biotite + Fe–Ti oxides as major mineral phases. Some samples contain amphibole glomerocrysts and clinopyroxene overgrowing biotite (Fig. 4b). Rare pseudoleucite phonolites occur in this unit as well. The samples of the CVU are often intensely altered.

The Syenitic Unit (SYU) comprises equigranular, phaneritic, medium to coarse-grained syenites and nepheline syenites (Fig. 4c–h). Several samples show a trachytoidal preferential alignment of feldspars. Major mineral phases are alkali feldspar + amphibole + biotite + clinopyroxene + Fe–Ti oxides ± nepheline ± plagioclase. Garnet is

rare but very prominent in the coarse grained (pegmatitic) rock varieties, where euhedral to subhedral brown garnet forms clusters with euhedral, black todark green amphibole. Accessory phases observed include zircon, titanite, fluorite, muscovite, apatite, calcite, sodalite and cancrinite. Subhedral alkali feldspar is typically the most abundant phase, frequently exhibiting significant alteration. Primary clinopyroxene commonly shows signs of incipient alteration to green amphibole.

5. Analytical methods

Major and trace elements were analysed by standard X-ray fluorescence (XRF), inductively coupled plasma atomic emission spectrometry (ICP-AES) and inductively coupled plasma mass spectrometry (ICP-MS) methods. Detailed information about the analytical methods used is provided in the supplementary material. Systematic differences between analyses from different laboratories are not observed. If they exist, they are likely to be small relative to the compositional effects of the magmatic processes operating, and considered negligible for the overall interpretation of the dataset.

Strontium (Sr) and neodymium (Nd) isotope analyses were performed at the School of Earth and Environment, University of Leeds. Conventional ion-exchange chromatographic techniques were applied and samples were analysed on a Thermo Finnigan Triton multicollector mass spectrometer (see Halama et al., 2013 for details of the analytical protocol). Information about reference materials analysed as well as normalisation and correction procedures applied is given in the supplementary material.

$^{40}\text{Ar}/^{39}\text{Ar}$ dating of amphibole from syenite sample 6–8–12 was performed using a CO₂ laser stepwise heating technique at the Institute of Earth and Environmental Science, Universität Potsdam. The analytical protocol follows established procedures and a brief summary about procedural aspects, standards used and corrections applied is provided in the supplementary material. Calculation of ages and errors was performed following Uto et al. (1997) using the total ^{40}K decay constant of $5.543 \times 10^{-10} \text{ a}^{-1}$.

6. Results

6.1. Rock classification and major element geochemistry

The Total Alkali versus Silica (TAS) diagram was used to classify the volcanic rocks from the OUV and CVU (Fig. 5a). For the intrusive rocks of the SYU, we used the classification diagram of De La Roche et al. (1980); Fig. 5b). Whole rock geochemical analyses are presented in Table 1. All volcanic rocks of the TAC are classified as alkaline in the TAS diagram (Fig. 5a). Rocks of the OUV cover a wide compositional range from basaltic trachyanandesite to phonotephrite, tephriphonolite and phonolite. The compositional range of the CVU rocks is more restricted, comprising trachyanedesites and trachytes. The plutonic rocks of the SYU are classified as nepheline syenites and syenites based on the R1 and R2 parameters (Fig. 5b), which generally agrees with the petrographic observations.

A further geochemical classification was carried out using various geochemical indices (Table 1) that allow an evaluation of petrogenetic relationships (Frost et al., 2001; Frost & Frost, 2008; Shand, 1947). The majority of the Tezhsar rocks are ferroan, alkalic, metaluminous and silica-undersaturated. The Alkalinity Index (AI; AI = Al-(K + Na) on a molecular basis) typically varies between 0 and 0.1, indicating that peralkaline rocks (AI < 0) are largely absent at the TAC. Values for the feldspathoid silica-saturation index (FSSI; normative Q-[Lc + 2(Ne + Kp)]/100, where Q = quartz, Lc = leucite, Ne = nepheline and Kp = Kalophilite) mostly range from -0.6 to 0. The negative FSSI values demonstrate that the rocks are generally silica-undersaturated. Diagrams using the aluminium-saturation index (ASI; molecular Al/(Ca-1.67P + Na + K) and the modified alkali-lime index (MALI; Na₂O +

Table 1

Table 1
Whole-rock geochemical data for samples from the Tezhsar Alkaline complex.

OVU	OVU	OVU	SYU											
2–12–09	2–13–09	3–2–09	1–4–15	2–1–15	2–8b–15	2–11–15	3–5–15	6–3–12	6–4–12	6–5–12	6–8–12	6–9–12	6–10–12	10–45–08
6	7	11	29	30	37	40	46	20	21	22	24	25	26	10
RHL	RHL	RHL	BV	BV	BV	BV	P	P	P	P	P	P	P	RHL
44.59755	44.59862	44.62817	44.58339	44.58454	44.58279	44.59697	44.57256	44.56770	44.56770	44.57538	44.59230	44.57735	44.58232	44.58325
40.64063	40.64185	40.65332	40.70836	40.70469	40.68375	40.69765	40.71180	40.68247	40.68247	40.68107	40.67115	40.69195	40.68042	40.63900
57.93	59.08	52.13	59.22	60.10	63.15	57.39	56.26	60.86	62.41	59.94	56.89	64.47	59.64	58.66
0.43	0.48	0.74	0.73	0.46	0.36	0.38	0.35	0.37	0.40	0.36	0.40	0.36	0.57	0.82
19.72	20.61	20.75	19.03	19.35	17.98	19.90	20.72	19.26	18.42	18.56	19.29	17.81	19.24	20.07
1.32	1.30	2.60	0.88	0.84	0.77	0.77	0.74	0.86	0.65	0.94	1.05	0.65	0.89	1.07
2.77	2.72	5.45	1.85	1.77	1.62	1.62	1.56	1.81	1.37	1.98	2.20	1.35	1.87	2.25
0.11	0.19	0.23	0.22	0.16	0.16	0.15	0.14	0.16	0.12	0.22	0.17	0.07	0.14	0.19
0.79	0.77	2.62	0.38	0.35	0.34	0.33	0.45	0.44	0.20	0.59	0.87	0.12	0.40	0.62
2.73	2.36	6.71	1.84	1.87	1.24	2.67	2.24	1.80	1.19	2.22	3.13	0.47	2.49	2.02
5.36	1.90	2.90	4.42	5.66	6.49	5.28	3.59	5.25	4.21	4.86	5.15	6.47	4.76	4.68
6.49	10.52	5.28	8.80	7.83	5.97	7.02	10.67	6.55	8.82	7.10	6.55	6.33	7.39	8.82
0.21	0.14	0.54	0.05	0.05	0.09	0.04	0.07	0.09	0.04	0.13	0.20	0.03	0.06	0.06
2.78	1.56	0.85	1.63	1.21	0.72	3.23	2.45	1.50	1.28	2.01	3.08	1.12	1.59	0.99
100.65	101.62	100.80	99.05	99.65	98.89	98.78	99.24	98.95	99.10	98.91	98.99	99.25	99.04	100.25
1110	3940	932	60	144	472	72	272	655	481	1030	891	87	150	208
6.23	7.35	18.1	13.1	12.7	30.2	77.2	13.1	na	na	na	na	na	na	7.4
2.89	3.96	26	bdl	bdl	bdl	bdl	bdl	21	bdl	12	14	12	bdl	3
1.34	1.7	5.88	4.8	3.4	4.3	4.7	9.8	na	na	na	na	na	na	2.23
na	na	na	18.7	20.9	21.7	19.5	14.2	19	20	19	20	23	19	na
3.24	3.01	2.14	11	11.7	22.4	11	3.4	21	bdl	12	14	12	bdl	6.27
10.5	11.4	6.95	75.1	61.7	49.5	45.9	16.2	41	59	32	31	45	56	55
137	193	186	233	235	261	247	452	251	305	257	197	303	236	175
2.75	1.85	13.1	bdl	bdl	bdl	bdl	bdl	1.7	1.3	3.7	4.2	2.9	2.1	1.64
na	na	na	2	2	1	bdl	na							
1230	3520	1280	885	330	384	2300	959	757	1030	1280	1710	42	1480	817
0.448	0.474	0.286	3.7	3.1	2.1	2.6	0.9	na	na	na	na	na	na	3.58
11.6	11.7	7.08	113	124	75.3	77.5	11.6	na	na	na	na	na	na	26.6
4.53	3.64	3.16	9.7	16.7	19.3	15.5	2.6	na	na	na	na	na	na	5.71
112	138	250	84	68	55	63	84	67	55	84	106	35	79	109
166	180	123	494	527	1080	629	168	737	1110	547	549	471	547	304
26.3	29.6	23.6	68.7	53	50.3	38	20.8	38	41	29	26	44	31	66
61.2	79.1	45.6	319	244	167	161	81	140	81	71	104	204	75	186
104	135	79.1	558	396	247	264	135	204	224	142	175	328	174	354
11.7	14.8	9.58	59.6	38.5	24.4	26.7	15	23	26	15	17	28	18	39.3
46.1	59.5	40	190	117	72.6	84.4	52.4	85	103	61	69	113	70	155
8.49	11.3	8.19	27.2	16.6	10.7	12.5	8.1	13	18	10	10	15	11	28.1
2.32	4.47	2.26	3.8	2.2	1.4	1.9	2.3	1.5	2.2	1.9	1.9	0.2	1.6	4.77
6.05	7.94	5.82	20.2	12.8	8.2	9.7	6.2	9.5	13	7.7	7.7	11	8	19.7
0.988	1.26	0.959	2.6	1.7	1.2	1.3	0.8	1.3	2.1	1.1	1.1	1.8	1.1	2.97
4.34	5.35	4.14	13.7	9.7	7.2	7.4	4	7.5	9.6	5.8	5.6	8.4	6	11.9
0.829	0.932	0.773	2.3	1.8	1.4	1.3	0.7	1.5	1.6	1.1	0.94	1.5	1.2	1.98
2.35	2.41	2.08	6.1	5.1	4.8	3.7	1.9	3.9	4.2	3	2.6	4.4	3.2	4.88
0.389	0.385	0.338	0.8	0.7	0.8	0.6	0.2	0.66	0.68	0.52	0.45	0.75	0.53	0.72
2.52	2.37	2.08	4.3	4.5	6	3.6	1.6	4	3.5	3	2.6	4.6	3.3	4.22
0.409	0.38	0.358	0.6	0.6	1	0.5	0.2	0.59	0.45	0.45	0.38	0.57	0.48	0.59
1.1	2.11	2.21	0.3	1.2	0.6	1.9	0.3	na	na	na	na	na	na	1.01
91.1	29.6	100	7.4	41.3	8.3	45.8	15	na	na	na	na	na	na	7.98
12.8	21.5	10.8	na	29.8										
na	na	na	13.1	4.7	18.4	22.4	1.7	97	63	110	83	49	80	na
67.9	95.7	120	48	13	65	34	17	na	na	na	na	na	na	92.9
1.27	3.48	13.6	0.1	0.4	0.5	0.5	0.2	na	na	na	na	na	na	4.56
0.704470	0.704057	0.704195								0.704341	0.704205		0.704647	0.704364
0.70429	0.70397	0.70395								0.70401	0.70401		0.70438	0.70401
	0.512851													0.512849
	0.512820													0.512820
	4.6													4.6
0.037	0.056	0.099	0.022	0.015	0.026	0.028	0.032	0.035	0.019	0.028	0.037	0.003	0.033	0.025
-0.11	0.37	-0.03	-0.1	-0.16	-0.03	-0.38	-0.25	0	0.79	-0.02	-0.12	1.12	-0.05	-0.17

(continued on next page)

Table 1 (continued)

SYU	SYU	SYU	SYU	SYU	CVU						
2–7-09	2–9-09	3–3-09	3–5-09	3–6-09	2–3-15	2–4-15	2–6-15	2–7-15	2–8a-15	3–7-09	3–8-09
1	3	12	14	15	32	33	35	36	37	16	17
RHL	RHL	K	RHL	K	BV	BV	BV	BV	BV	RHL	RHL
44.59320	44.59835	44.62075	44.61660	44.61053	44.58697	44.58697	44.58893	44.58929	44.58279	44.60143	44.60703
40.63365	40.63848	40.65353	40.66855	40.67683	40.69464	40.69464	40.69384	40.69375	40.69033	40.67552	40.67572
56.21	51.44	55.14	58.89	60.17	59.14	57.81	55.77	63.47	61.08	60.21	61.49
0.11	0.47	0.36	0.44	0.37	0.37	0.36	0.43	0.32	0.34	0.34	0.36
22.61	20.65	21.91	20.96	19.05	20.13	19.49	21.71	19.61	18.56	20.00	19.63
0.72	1.48	0.65	0.96	0.77	0.99	0.97	0.82	0.53	0.99	1.03	0.95
1.52	3.10	1.37	2.02	1.62	2.07	2.04	1.72	1.11	2.08	2.16	2.00
0.28	0.18	0.22	0.12	0.17	0.18	0.17	0.20	0.05	0.18	0.17	0.16
0.04	0.91	0.16	0.29	0.46	0.70	0.75	0.45	0.27	0.63	0.52	0.42
1.49	4.03	2.13	2.24	2.26	1.85	3.04	3.24	0.17	2.71	2.38	1.92
9.51	4.68	7.63	4.83	5.48	4.95	5.34	7.04	5.91	6.70	6.27	6.25
6.52	9.73	7.94	7.45	6.79	6.97	6.35	3.63	7.57	4.56	6.53	6.79
0.01	0.20	0.03	0.06	0.08	0.15	0.13	0.08	0.04	0.12	0.08	0.07
1.77	2.44	1.15	2.66	1.44	1.84	2.06	4.32	0.88	0.79	1.19	na
100.79	99.31	98.69	100.92	98.66	99.34	98.51	99.41	99.93	98.74	100.88	100.04
9.31	4490	na	170	530	909	906	787	201	1430	546	388
1.55	7.96	na	5.61	na	20.9	43.1	11.3	12.8	4.6	4.81	4.3
2.98	2.55	na	4.24	na	bdl	bdl	bdl	bdl	8.56	11.7	
5.56	2.92	na	6.38	na	5	5.8	1.3	1.1	5	7.36	6.59
na	na	na	na	na	20.2	20.5	19	22.6	19	na	na
10.9	4.2	na	11.1	na	11.2	11.5	4.5	16.4	11.6	13.2	10.5
8.2	18	na	54.4	na	31.5	33.6	19.6	43.2	31	41.8	36.4
407	227	na	226	203	227	205	169	251	183	249	232
0.759	1.04	na	1.04	na							
na	na	na	na	na	1	1	bdl	2	1	bdl	bdl
50.6	5270	na	573	506	861	1990	984	515	1480	855	403
0.00647	0.752	na	3.12	na	1.4	1.5	0.9	1.8	1	1.71	1.67
31.1	15.4	na	85.5	na	45.4	48.9	24.1	109	60.4	59.6	45.4
10.4	5.73	na	12.7	na	12.1	17.6	3.6	19.9	19.1	19.7	14.6
14.1	230	na	71.9	na	90	89	201	242	82	71.3	66.4
856	273	na	677	na	568	612	284	810	487	723	575
12.3	38.1	na	34.3	na	31.9	31.3	53.9	19	28.4	37.4	37.3
169	96.7	na	191	138	137	114	181	57.3	94.1	133	121
187	171	na	285	220	184	177	246	79	150	204	195
12	18.6	na	25.5	21.4	19.1	17	29.8	11.3	14.5	18.4	18.6
26.3	74.5	na	85	68.1	61.3	55.1	102	36.2	47	62.9	66.6
2.35	14.5	na	13.2	10.8	8.9	8.2	16.1	6.2	7	10.3	11.4
0.338	5.16	na	2.14	2.09	2.1	1.9	4.5	1.1	1.7	2.05	2.22
3.22	10.6	an	10.4	8.85	7	6.5	14	4.1	5.5	8.09	8.73
0.295	1.7	na	1.45	1.18	0.9	0.9	1.7	0.6	0.8	1.25	1.31
1.17	7.04	na	5.91	6.23	5.2	5	9.1	3.5	4.4	5.49	5.81
0.291	1.19	na	1.06	1.17	1	0.9	1.5	0.6	0.8	1.06	1.08
1.1	2.94	na	2.86	3.25	2.8	2.9	4.1	2.2	2.6	3.08	3.02
0.229	0.434	na	0.454	0.488	0.4	0.5	0.6	0.4	0.4	0.561	0.529
1.67	2.64	na	2.73	3.33	3.1	3.2	3.7	2.9	3.1	3.93	3.61
0.365	0.398	na	0.403	0.479	0.5	0.5	0.5	0.5	0.5	0.621	0.582
1.11	1.6	na	1.72	na	0.6	3.7	1.2	2.2	0.3	1.44	2.59
2.33	20.7	na	70.4	na	32	21.1	19	3.2	17.9	29.5	18
66.3	17.7	na	20.9	na	na	na	na	na	25	38.5	
na	na	na	na	na	20.5	25.2	4.2	20.4	13.7	na	na
181	104	na	77.3	85	60	51	61	55	37	100	88.7
0.796	2.87	na	3.33	16	2.3	0.6	0.5	0.6	0.6	0.881	1.7
0.718557	0.704075	0.706855	0.704695	0.704873						0.704519	0.704987
0.70520	0.70400	0.70424	0.70404	0.70414						0.70404	0.70403
		0.512837									
		0.512813									
		4.4									
−0.003	0.021	0.005	0.047	0.025	0.044	0.038	0.061	0.017	0.026	0.023	0.017
−0.63	−0.55	−0.55	−0.07	−0.07	−0.02	−0.11	−0.16	−0.01	−0.03	−0.16	−0.13

* Fe₂O₃ and FeO contents were calculated based on a Fe³⁺/Fe_{Total} ratio of 0.3.

Abbreviations: BV = Bureau Veritas, P = Potsdam, RHL = Royal Holloway London, K = Kiel; na = not analysed; bdl = below detection limit

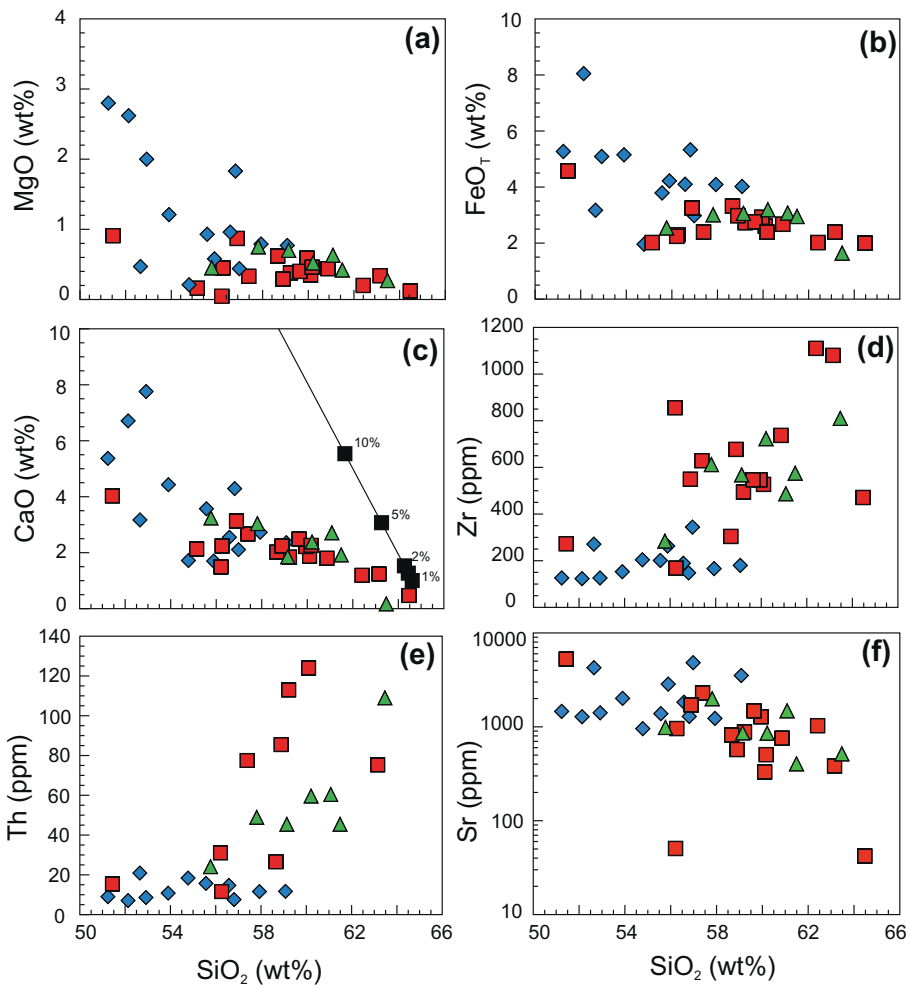


Fig. 6. Harker diagrams of the TAC samples for selected major (a-c) and trace (d-f) elements. The limestone assimilation trend in (c) was calculated after Costa et al. (2013) using limestone composition WGZ-3 from Zhang et al. (2017). All symbols as in Fig. 5.

K₂O-CaO) classification demonstrate the predominantly metaluminous and alkalic nature of the TAC rocks (Fig. 5c, d). Peraluminous compositions (ASI > 1) are very rare. Compared to the restricted compositions of SYU and CVU, the OVU shows the largest variations in A/NK ratios.

Harker diagrams show a relatively smooth decrease of MgO, total FeO (FeO_T) and CaO with increasing SiO₂ contents (Fig. 6a-c). MgO contents are below 3 wt% for OVU rocks and SYU and CVU rocks have <1 wt % MgO, demonstrating their highly evolved character and suggesting substantial fractionation of mafic minerals prior to crystallization.

6.2. Trace element geochemistry

Whole-rock trace element concentrations in the TAC are variable and show some significant enrichment in Sr (up to ~5000 ppm), Ba (up to ~4000 ppm), Zr (up to ~1000 ppm) and ΣREE (up to ~1200 ppm), which is typical for alkaline igneous rocks (Chakhmouradian & Zaitsev, 2012). Incompatible trace elements such as Th and Zr show pronounced enrichment with increasing silica, in particular evident for SYU and CVU rocks (Fig. 6d, e). In contrast, Sr contents remain relatively constant for intermediate rocks with <58 wt% SiO₂ and diminishing at higher silica contents (Fig. 6f). A chondrite-normalised REE diagram (Fig. 7a) shows that both the volcanic and plutonic rocks of the TAC are characterized by a strong fractionation between LREE and HREE with La_(N)/Yb_(N) ratios predominantly around 10–40 but reaching values as high as 70. Absolute amounts of LREE are generally higher in the SYU (~200–1000 x chondrite) compared to the OVU and CVU

(~40–500 x chondrite). Europium anomalies, defined as Eu/Eu* = $\frac{Eu_N}{\sqrt{(Sm_N \times Gd_N)}}$, are moderately negative in the volcanic units OVU (0.80–1.08) and CVU (0.68–0.91). The majority of the SYU rocks have more pronounced negative Eu anomalies with Eu/Eu* values between 0.44 and 0.97 (Fig. 7a). On primitive mantle-normalised trace element diagrams (Fig. 7b-d), negative anomalies for Nb, Ta and Ti are the most prominent features in all three units. In contrast, a strong relative enrichment of Th and U compared to Rb and Ba is only significant in the SYU and CVU, but not discernible in the OVU.

6.3. Sr and Nd isotopes

Initial Sr and Nd isotope ratios of volcanic and plutonic rocks from the TAC, recalculated to an age of 41 Ma, range from 0.7040 to 0.7052 and 0.51274 to 0.51283, respectively (Table 1). 19 of 20 samples fall within the range 0.7040 to 0.7044 for the initial ⁸⁷Sr/⁸⁶Sr ratio. The Nd isotopic compositions correspond to positive εNd values between +3.0 and +4.8 (Table 1).

6.4. ⁴⁰Ar/³⁹Ar geochronology

One syenite sample (sample number 6-8-12) was dated by ⁴⁰Ar/³⁹Ar step heating. The total gas age is 42.1 ± 0.5 Ma (Fig. 8; Table 2). We use the following criteria outlined by Fleck et al. (1977) for defining a plateau age: (1) The plateau includes at least 50% of the total ³⁹Ar released, (2) the ages of two contiguous steps in the plateau agree

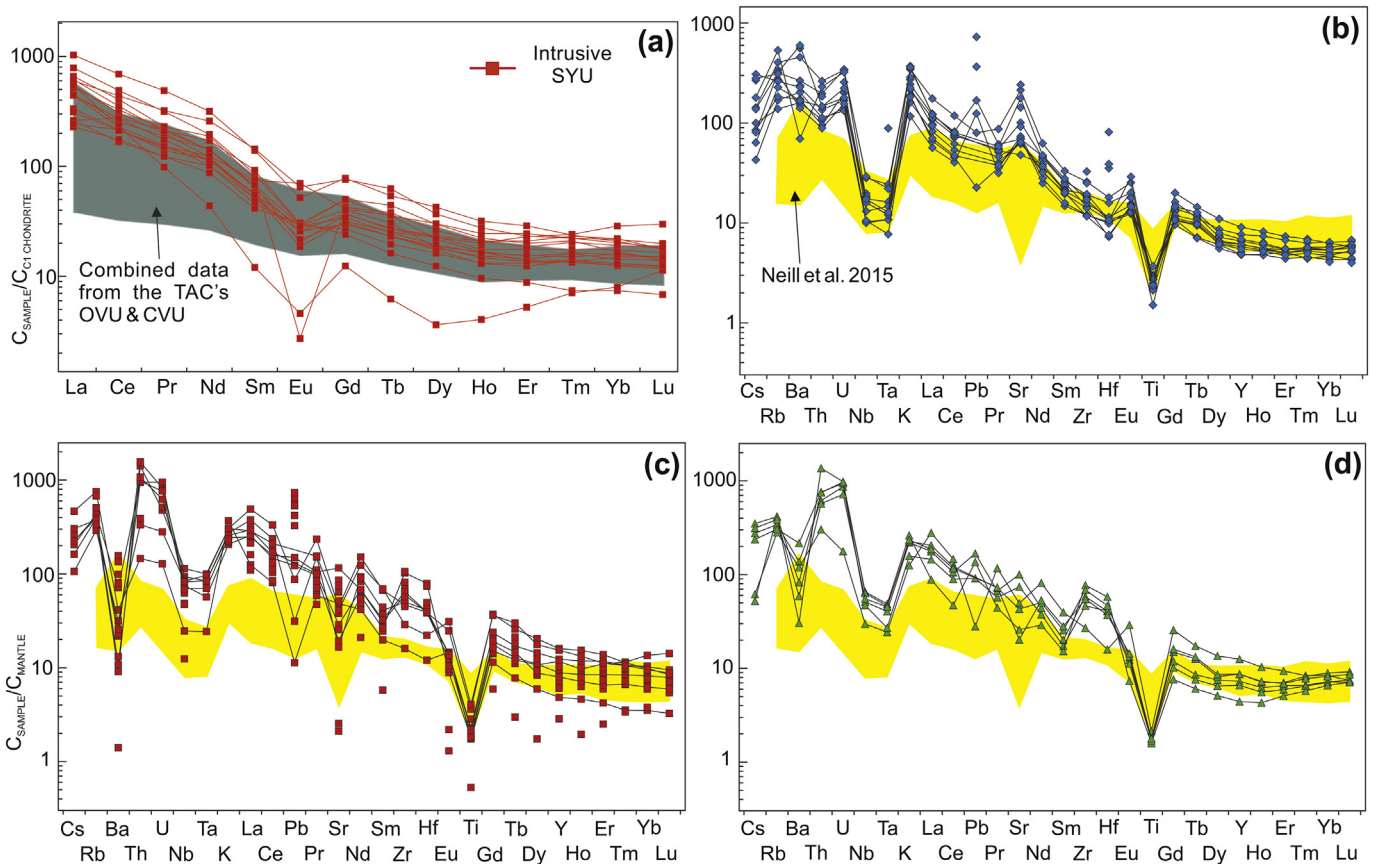


Fig. 7. (a) Chondrite-normalised REE diagram highlighting more pronounced LREE fractionation and negative Eu anomalies within the SYU relative to the volcanic units of the TAC. Normalisation values from Boynton et al. (1984). (b-d) Mantle-normalised trace element diagrams of rocks from the TAC; (b) – OJV, (c) – SYU, (d) – CVU. Normalisation values after McDonough & Sun, 1995. Comparative data from Neill et al. (2015) for Pliocene-Quaternary volcanic rocks from central and northern Armenia.

within 2 s error, excluding the J value error, (3) the plateau consists of three steps or more, and (4) each degassing step contributing to the plateau contains >3% of the total ^{39}Ar released. For the syenite sample 6–8–12, five plateau steps constituting 98.88% of the total ^{39}Ar released can thus be used to define a plateau age of 41.0 ± 0.5 Ma (Fig. 8; Table 2). Using the plateau steps only, a normal isochron age of 41.3 ± 2.5 Ma with a $^{40}\text{Ar}/^{36}\text{Ar}$ intercept at 281 ± 58 is obtained. The corresponding inverse isochron yields an age of 41.2 ± 2.1 Ma with $(^{40}\text{Ar}/^{36}\text{Ar})_i = 289 \pm 57$. The good agreement between the three ages underlines the reliability of the age determination, with the plateau age of 41.0 ± 0.5 Ma representing the most precise and hence preferred age.

7. Discussion

7.1. Comparison with regional magmatic signatures

The alkaline and highly evolved nature of the TAC rocks makes them distinct from volcanic rocks outcropping in Armenia, which are typically transitional between alkaline and subalkaline. This includes the trachybasaltic to trachyanedesitic Pliocene-Quaternary rocks from northern Armenia (Neill et al., 2013, 2015), as well as rocks from the large polygenetic Aragats volcano (Connor et al., 2011) and from the Gegham, Vardenis and Syunik Volcanic Highlands in South Armenia (Karapetian et al., 2001; Sugden et al. submitted). A comparison with data for regionally related Miocene to Quaternary Armenian igneous rocks from the Yerevan and Shirak regions (Neill et al., 2015) reveals a general enrichment of the TAC rocks in almost all moderately to highly incompatible trace elements (Fig. 7b-d). Key features, such as negative Nb-Ta and Ti anomalies and a relative enrichment of LREE compared to HREE, are similar. Isotopically, the TAC rocks, which plot on the Sr–Nd mantle array, overlap with plutonic rocks from the Meghri-Ordubad pluton and with other Miocene to Quaternary volcanic rocks from Armenia (Fig. 9). Quaternary volcanic rocks from Aragats (Connor et al., 2011; Lebedev et al., 2007) and the Gegham Ridge (Lebedev et al., 2013) also overlap in their Sr–Nd isotopic compositions. This comparison reveals that there is a broad Sr–Nd isotopic homogeneity across a large area of the Armenian highlands from the Eocene to the Quaternary, indicating that similar source regions are involved in magma genesis. Broadly contemporary (47–40 Ma) post-collisional magmatic rocks from the Eastern Pontides (NE Turkey), which are characterized by tholeiitic/calc-alkaline affinities enriched in LILE with pronounced depletions in HFSE, also overlap in their isotopic composition

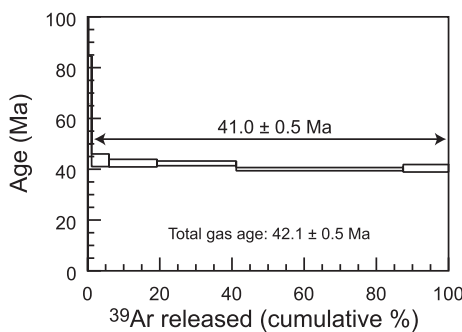


Fig. 8. $^{40}\text{Ar}/^{39}\text{Ar}$ age spectrum plot for the amphibole separate from syenite sample 6–8–12.

Table 2

Argon isotopic data for an amphibole separate of syenite sample 6–8–12.

TZ-6-8-12	Laboratory ID: C15038	Irradiation ID: PO-2	$^{40}\text{Ar}/^{39}\text{Ar}$	$^{37}\text{Ar}/^{39}\text{Ar}$	$^{36}\text{Ar}/^{39}\text{Ar}$ ($\times 10^{-3}$)	K/Ca	$^{40}\text{Ar}^*$ (%)	$^{39}\text{Ar}_\text{K}$ fraction (%)	$^{40}\text{Ar}^*/^{39}\text{Ar}_\text{K}$	Age (Ma)	\pm	1 s	
J = 0.0009720													
Laser output													
1.8%	1397	\pm 251	7.4	\pm 137	3703	\pm 711	0.08	21.73	0.13	305	\pm 98	469	\pm 132
2.0%	1385	\pm 938	141	\pm 566	4558	\pm 3110	0.00	3.54	0.03	54	\pm 147	93	\pm 245
2.4%	352	\pm 60	6	\pm 149	919	\pm 203	0.10	22.92	0.14	81	\pm 44	137	\pm 71
2.8%	77	\pm 3	39	\pm 15	141	\pm 33	0.01	49.59	0.82	39	\pm 10	67	\pm 17
3.1%	37.0	\pm 0.4	7	\pm 4	42	\pm 5	0.09	67.55	4.85	25.1	\pm 1.4	44	\pm 2
3.3%	29.79	\pm 0.16	6	\pm 2	20	\pm 3	0.10	81.79	13.29	24.5	\pm 0.9	42.4	\pm 1.5
3.5%	29.80	\pm 0.14	1.6	\pm 1.7	18.7	\pm 1.7	0.37	81.82	21.93	24.4	\pm 0.5	42.3	\pm 0.9
3.7%	30.8	\pm 0.2	2.4	\pm 0.6	26.9	\pm 1.0	0.25	74.79	46.26	23.1	\pm 0.4	40.0	\pm 0.6
3.9%	31.1	\pm 0.4	2.4	\pm 1.9	27	\pm 3	0.25	74.67	12.56	23.3	\pm 0.9	40.4	\pm 1.5
Total gas age												42.05	\pm 0.52
Plateau age (step 5–9: 98.8% of total ^{39}Ar)												40.96	\pm 0.46
Normal isochron age (step 5 to 9)												41.32	\pm 2.51
Inverse isochron age (step 5 to 9)												41.25	\pm 2.11

(Aydinçakır & Şen, 2013). In contrast, extending the comparison to Eocene magmatic rocks in NW Iran reveals that post-collisional granites and syenites from the Sanandaj–Sirjan Zone and granitoids from the Urumieh–Dokhtar magmatic arc extend to significantly more radiogenic Sr–Nd isotope compositions (Fig. 9).

7.2. Magma differentiation and magma source geochemistry

Both volcanic and plutonic rocks of the TAC are evolved and only a few samples are of intermediate composition (Fig. 5a, b). The influence of mixing, fractional crystallization and batch partial melting on the bulk geochemical composition of the rocks can be evaluated using incompatible trace elements with different bulk solid/liquid partition coefficients

(Schiano et al., 2010). In the Rb/Nd vs. Rb diagram (Fig. 10a), the near-horizontal trend for the majority of data points emphasizes the dominant role of fractional crystallization, whereas mixing and differences in batch partial melting would yield positive correlations (Schiano et al., 2010). This interpretation is supported by a curved overall trend in the Rb vs. Rb/V diagram (Fig. 10b), which is consistent with fractional crystallization or mixing, but not with different degrees of partial melting (Schiano et al., 2010). Moreover, the coherent trend of the Rb/Ba vs. Ba diagram (Fig. 10c) reflects feldspar fractionation and does not indicate any significant effects of hydrothermal alteration. A major role of the role of crustal contamination processes can also be excluded based on the unradiogenic initial $^{87}\text{Sr}/^{86}\text{Sr}$ isotope ratios that remain relatively constant with increasing silica (Fig. 10d). Crustal contamination

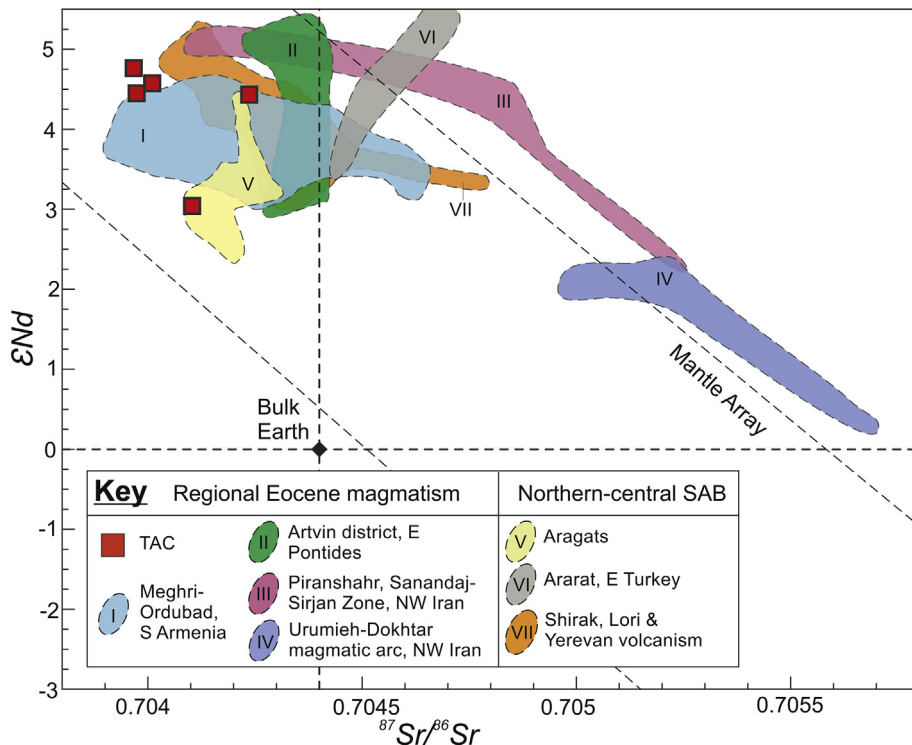


Fig. 9. Sr–Nd isotope diagram of the TAC data (red squares) in comparison to other Eocene–Quaternary igneous rocks in the Lesser Caucasus and adjacent regions. The mantle array is from Lebedev et al. (2007) after DePaolo & Wasserburg (1979). Data sources: (I) – Moritz et al. (2016); (II) – Aydinçakır & Şen (2013); (III) – Kazemi et al. (2018); (IV) – Mazhari et al. (2009); (V) – Connor et al. (2011); (VI) – Kheirkhah et al. (2009); (VII) – Neill et al. (2013, 2015). Literature data were recalculated using the ^{87}Rb decay constant of $1.3972 \times 10^{-11} \text{ a}^{-1}$.

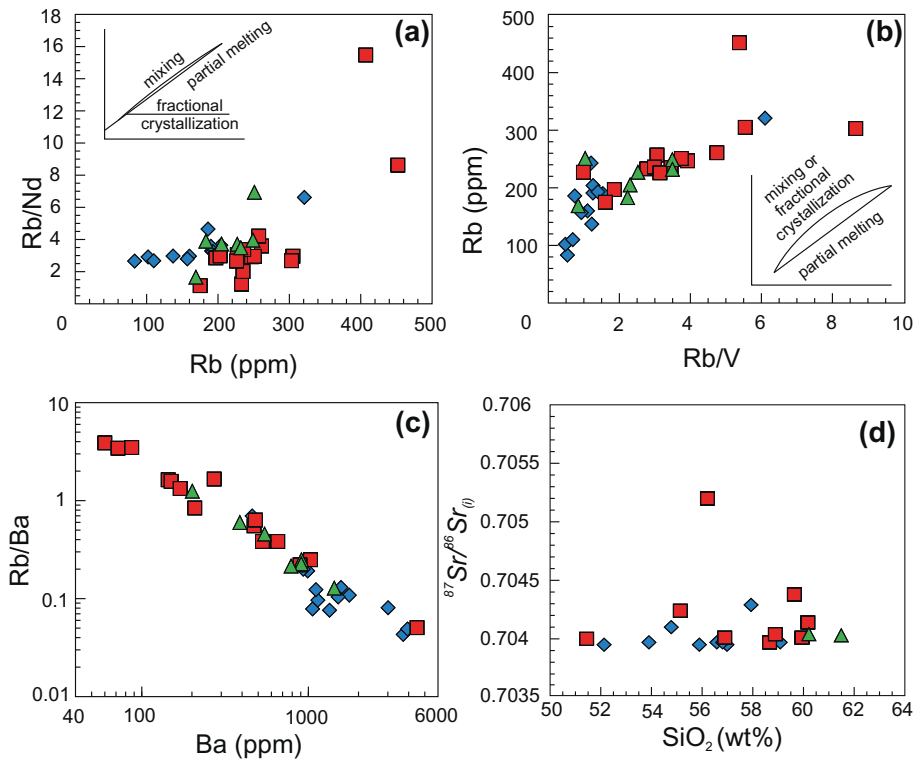


Fig. 10. TAC samples plotted in various diagrams to evaluate effects of distinct magmatic processes. (a) Rb/Nd vs. Rb diagram (after Schiano et al., 2010) where horizontal trends reflect fractional crystallization and positive correlations can be caused by mixing or batch partial melting. (b) Rb vs. Rb/V diagram (after Schiano et al., 2010) where curved trends, as observed for the TAC rocks, reflect fractional crystallization or mixing. (c) Rb/Ba vs. Ba diagram exhibiting a smooth trend indicative of feldspar fractionation. (d) Initial $^{87}\text{Sr}/^{86}\text{Sr}$ isotope ratios of the TAC samples plotted against SiO_2 content. All samples except one plot in a very narrow range of ($^{87}\text{Sr}/^{86}\text{Sr}$)_i ratios and there is no clear trend with increasing SiO_2 content. The sample with the elevated ($^{87}\text{Sr}/^{86}\text{Sr}$)_i ratio (2-7-09) has a high Rb/Sr ratio of ~8 and might be affected by post-magmatic Rb and/or Sr mobilization and a larger uncertainty in recalculation.

typically leads to an coupled increase in ($^{87}\text{Sr}/^{86}\text{Sr}$)_i and SiO_2 , which is not observed for the TAC. The only sample with an elevated ($^{87}\text{Sr}/^{86}\text{Sr}$)_i ratio (2-7-09) has a high Rb/Sr ratio of ~8 and might be affected by a larger uncertainty in recalculation of the initial value and/or post-magmatic Rb or Sr mobilization. There is also no indication of limestone assimilation, which would lead to a significant enrichment in CaO (Fig. 6c).

Olivine is conspicuously absent in all TAC rocks, but the low MgO contents and the highly evolved character point to preceding fractionation of mafic minerals (Fig. 6). The decrease in CaO/Al₂O₃ coupled with increasing FeO_t/MgO ratios, Eu anomalies that become more negative with increasing degree of differentiation, and decreasing Sr contents and Dy/Yb ratios with increasing SiO_2 suggest a significant role of amphibole/clinopyroxene and plagioclase fractionation whereas garnet fractionation was insignificant (Fig. 11a–c). Typically, the OUV rocks are more primitive than both CVU and SYU rocks. OUV rocks even retain Eu/Eu* values close to 1, pointing to lack of significant plagioclase fractionation (Fig. 11b).

The pronounced depletions in HFSE (Nb, Ta, and Ti) in all TAC rocks emphasizes the influence of subduction processes on the mantle source (Fig. 7). Similar negative HFSE anomalies have been observed in alkaline rocks of the Longbaoshan Complex, North China Craton (Lan et al., 2011) and carbonatites from east Tibet in the Himalayan collision zone (Hou et al., 2006) and were attributed to subduction processes influencing the magma source regions prior to continental collision. In addition, various trace element indicators for source enrichment processes support the notion that the OUV and the CVU are geochemically distinct (Fig. 11d–f). The OUV shows elevated Sm/Yb and Ba/La ratios, as well as relatively low La/Sm and Th/Yb ratios compared to the CVU (Fig. 11d–f). Collectively, these geochemical features of the OUV are interpreted as a signature of moderate fluid enrichment via slab dehydration inherited from earlier subduction events. Both CVU and OUV

rocks share high Ba/Nb ratios, similar to arc volcanic rocks in general (Fig. 12a). There is little overlap between the two groups as OUV rocks are additionally characterized by, on average, higher La/Nb ratios and Ba/Nb ratios >100, suggesting a temporal evolution towards a decreasing subduction influence from the early OUV to the late stage CVU. The more scattered trend towards lower Ba/Nb ratios in the syenites and nepheline syenites is likely a result of progressive alkali feldspar fractionation and should not be considered as the parental magma signature. The felsic plutonic rocks from the SYU tend to exhibit a larger geochemical variability when compared with the volcanic rocks, which is likely related to the fact that some show cumulate textures and may not represent melt compositions. The CVU, in contrast, has compositions that are more tightly clustered, with a faint indication of source enrichment from subducted sediments. Mechanisms of enrichment of the mantle source can be distinguished using [Hf/Sm]_N and [Ta/La]_N ratios (Fig. 12b), where TAC rocks are characterized by a subduction metasomatism signature, clearly distinct from carbonatitic metasomatism.

Sr–Nd isotopic compositions are broadly overlapping with Eocene to Pliocene magmas from the Meghri-Ordubad pluton and Pliocene to Quaternary volcanism in central and northern Armenia, pointing to only minor spatial variations in the respective mantle source regions (Fig. 10). The source of the TAC magmas is dominated by a depleted mantle component and crustal contamination is essentially absent, as all of the possible crustal contaminants would greatly enhance the radiogenic isotope signatures of the magmas, which is not the case. Silica-undersaturated alkaline rocks commonly have isotopic compositions that suggest a magma source in the mantle (Dunworth & Bell, 2001; Kramm & Kogarko, 1994). For instance, nepheline syenites from the Gardar Province (Greenland) show Nd isotopic compositions typical for mantle-derived rocks without any significant crustal assimilation (Halama et al., 2005; Marks et al., 2004). Therefore, evolved silicate

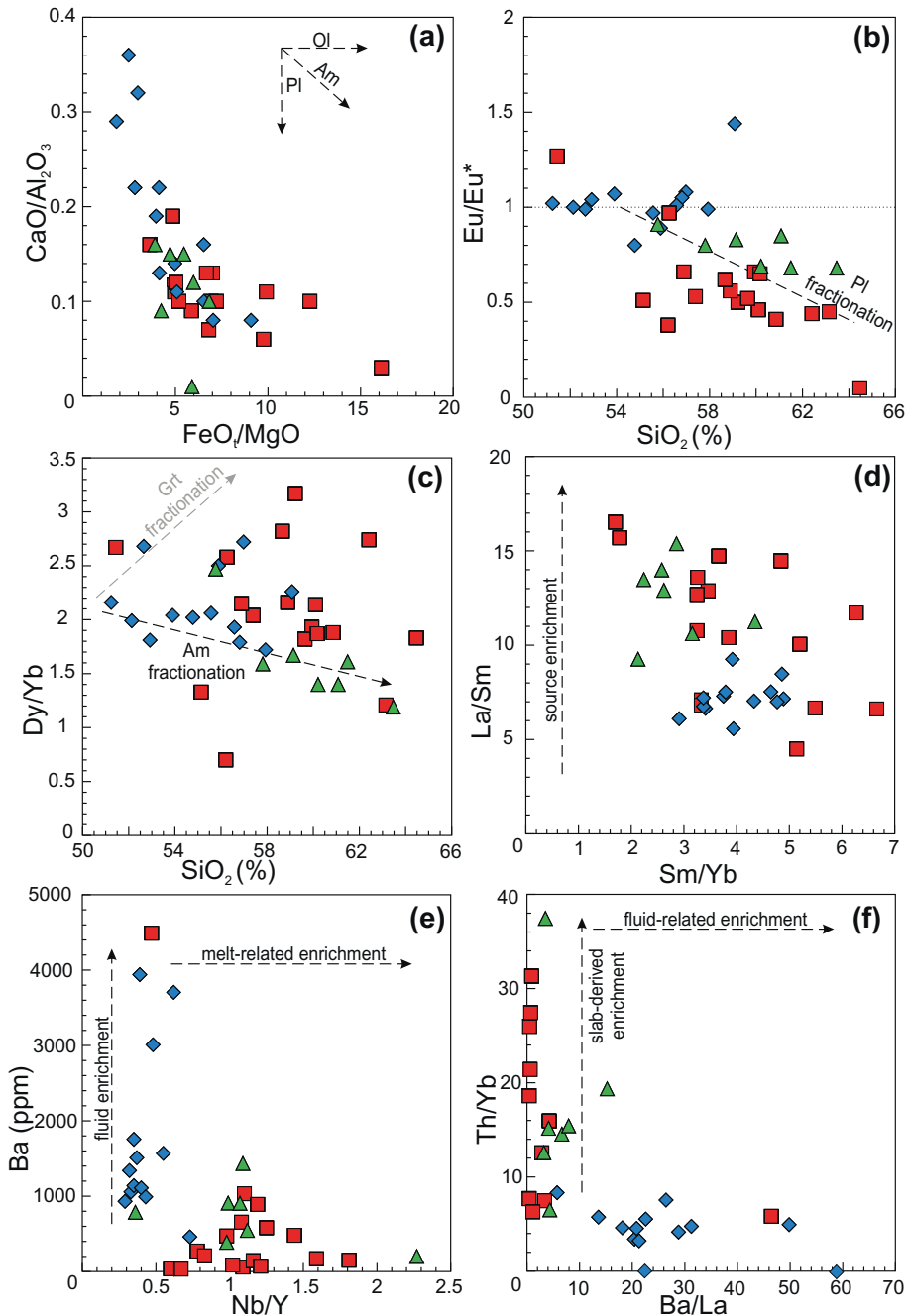


Fig. 11. Major and trace element indicators for fractionation and source enrichment processes. (a) $\text{CaO}/\text{Al}_2\text{O}_3$ vs FeO_t/MgO diagram showing fractionation trends for plagioclase, olivine and amphibole(am)/clinopyroxene(cpx) after Moritz et al. (2016). (b) Eu/Eu^* vs SiO_2 diagram depicting negative Eu anomalies in SYU and CVU samples, indicating plagioclase fractionation. (c) Dy/Yb vs SiO_2 diagram with fractionation trends for garnet and amphibole after Davidson et al. (2007). (d) La/Sm vs Sm/Yb diagram with approximate mineral stability thresholds of in mantle melt residues after Mamani et al. (2010). Note the distinct signatures for the two volcanic units of TAC. (e) Ba vs Nb/Y diagram displaying trends for fluid enrichment due to slab dehydration and mantle-derived melt enrichments after Keppezhinskaya et al. (1997). Slab fluid enrichment is prominent in the OVV rocks. (f) Th/Yb vs Ba/La diagram with trends for enrichment from subducted slab sediments and slab fluids from Woodhead et al. (2001). Elevated Ba/La ratios in OVV rocks suggest source enrichment via slab fluids.

undersaturated rocks are interpreted as products of differentiation from more primitive nephelinic, basanitic or alkali basaltic magmas derived from the upper mantle (Kramm & Kogarko, 1994; Trumbull et al., 2003). Basanitic volcanism is common to the south of TAC in the Syunik Volcanic Highland (Sugden et al. submitted) near the Armenia-Azerbaijan-Iran border region.

The trace element evidence for a subduction modifications and the Sr—Nd isotopic evidence for previous melt extraction suggest that the TAC magmas are predominantly derived by low degrees of partial melting from a lithospheric mantle source which has been affected by pre-

Eocene subduction i.e., prior to post-collisional melt generation. This magma generation model is also the preferred model for volcanism in East Anatolia (Keskin, 2003), and similar geochemical features in volcanic rocks from the Eastern Pontides (Artvin Province) contemporary (47–40 Ma) to emplacement of the TAC were also interpreted to be derived from a mantle source that had experienced metasomatism by slab-derived fluids (Aydinçakır & Sen, 2013). Post-collisional magmatic processes are commonly affected by prior subduction processes and LILE-enriched mantle sources are characteristic for these rocks (Bonin et al., 1998), typically resulting in calc-alkaline magmatic suites

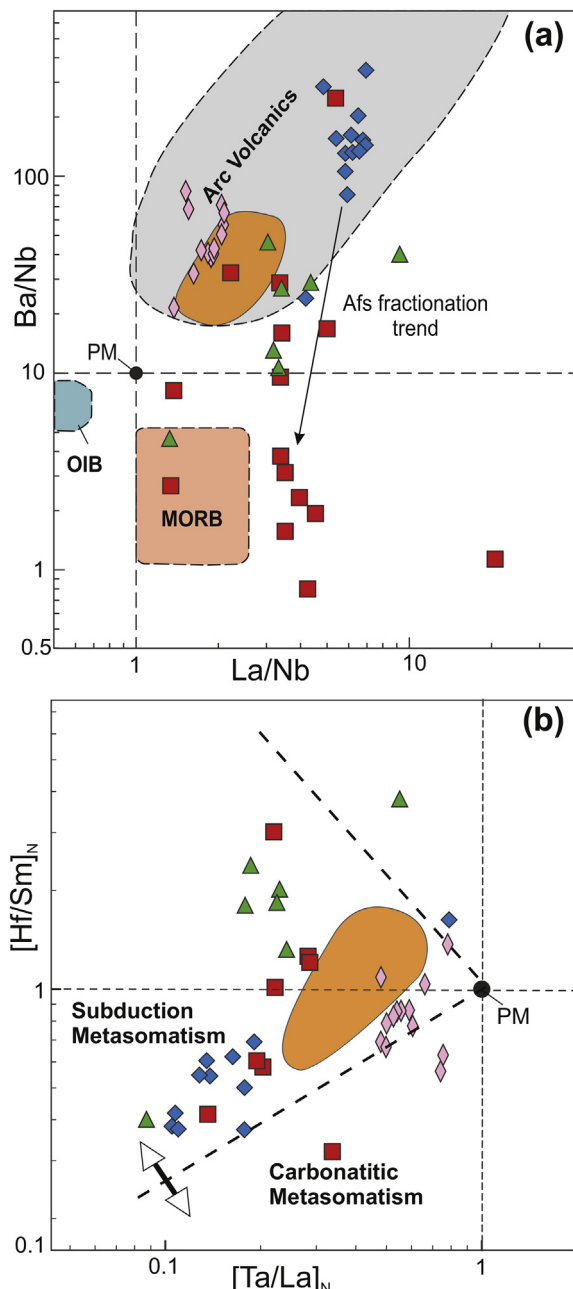


Fig. 12. Trace element ratio diagrams of TAC rocks. (a) Ba/Nb vs La/Nb. Alkali feldspar fractionation trend highlighted as a result of Ba depletion. Field boundaries after Jahn et al. (1999). (b) (Ta/La)_N vs (Hf/Sr)_N. Influence of subduction metasomatism is suggested by strongly decreasing (Ta/La)_N ratios. Field boundaries after La Flèche et al. (1998). Comparative data for Eocene magmatic rocks from the Talysh mountains, Azerbaijan (Vincent et al., 2005 – pink diamonds) and Pliocene–Quaternary volcanic rocks from central and northern Armenia (Neill et al., 2013, 2015 – orange field).

(Harris et al., 1986). The TAC represents an unusual case insofar as the post-collisional magmatic rocks are alkaline in character but also derive from a subduction-modified mantle source.

7.3. The age of the Tezhsar Alkaline complex in a regional context

The mid-Eocene age of 41.0 ± 0.5 Ma falls into a time of widespread magmatism in the Lesser Caucasus region, which lasted from ~49 to ~38 Ma and comprised the emplacement of alkaline and nepheline-bearing gabbros, monzonites and syenites as well as gabbro-diorite-

granodiorite-syenogranite complexes and granites (Ghukasyan et al., 2006; Melkonyan et al., 2008; Moritz et al., 2016). The magmatic activity was accompanied by porphyry-type Cu–Mo mineralization that was dated at 44–40 Ma by Re–Os analyses of molybdenite (Moritz et al., 2016). Slightly younger alkaline magmatism is represented by the Bunduk alkaline complex (38–32 Ma) located ~15 km northeast of the TAC (Magakyan 1981; Meliksetian, 1989). This pluton intrudes the Middle-Late Eocene volcanic suite of the Bazum ridge and the Bazum gabbro-granitoid intrusive complex, exhibiting an elongate morphology, parallel to the segment of Pambak-Sevan fault.

Regionally, broadly contemporaneous magmatic activity is also recorded in the Talysh mountain range (Azerbaijan/Iran) at around 41–38 Ma (Vincent et al. 2005), in the Eastern Pontides (Turkey) at ~46–40 Ma (Aydinçakır & Şen, 2013) and in western Georgia at ~47–41 Ma (Lebedev et al., 2009). Further to the SE in the Zagros orogen, ~41 Ma old granites and syenites occur in the Piranshahr massif (Mazhari et al., 2009) and ~40 Ma granitoids in the Urumieh-Dokhtar arc (Kazemi et al., 2018). The peak of subduction-related magmatism in Iran is also close to 40 Ma (Allen & Armstrong, 2008), and a magmatic flare-up lasting ~18 million years from 55 to 37 Ma has been postulated in the Urumieh-Dokhtar belt and the Alborz Mountains in Iran (Verdel et al., 2011). Throughout the Eocene, the plate convergence between the Arabian and Eurasian plates was proceeding at rates of 2–3 cm/year (McQuarrie et al. 2003). Following the initiation of the Arabia-Eurasia collision, arc magmatism declined in the Late Eocene (Allen & Armstrong, 2008). However, convergence was relatively rapid throughout Eocene–Oligocene time, and only slowed since Early Miocene (Rosenbaum et al., 2002).

The age of the TAC falls within this period of extensive magmatism during convergence between the Arabian and Eurasian plates, and its geochemical characteristics demonstrate a subduction-related origin. This subduction signature is inherited from prior northward subduction of the Neotethys ocean underneath the Eurasian margin, leading to a preconditioning of the mantle (Verdel et al., 2011). Typical calc-alkaline, subduction-related Eocene magmatism typical for active arc environments is preserved in the oldest granitoids (49–44 Ma) of the Meghri-Ordubad pluton (Moritz et al., 2016). The Lesser Caucasus experienced extension and crustal thinning at around 40 Ma causing decompression melting of the hydrated, subduction-influenced lithospheric mantle (Verdel et al., 2011), which imparted its geochemical signature onto the TAC magmas. Middle Eocene (ca. 49–40 Ma) extension, accompanied by magmatism, also occurred in Iran (Ballato et al., 2011). The extension-related magmatism in an overall setting of convergence (Rosenbaum et al., 2002) is caused by the rollback of the Neotethys slab (Verdel et al., 2011; Vincent et al. 2005).

The oldest rocks at TAC in the OVV show some geochemical characteristics reminiscent of a dehydration fluid signature in arc magmatic rocks (high Ba/Nb, Ba/La ratios; Figs. 7 and 11e, f). A clear arc signature, most evident in the pronounced negative Nb–Ta anomalies, is present in all of the TAC rocks, similar to the Meghri-Ordubad pluton at the Armenia-Iran border. However, the TAC rock compositions are distinct as they are not calc-alkaline but alkaline (Fig. 5) with a pronounced enrichment in incompatible trace elements (e.g. up to 5000 ppm Sr and typically 100–500 ppm Rb compared to <1000 ppm Sr and 10–200 ppm Rb in rocks from Meghri). This geochemical character is not due to long-lived differences in the mantle source compared to Meghri-Ordubad pluton since the Sr–Nd isotopic characteristics are similar (Fig. 9). Instead, smaller degrees of melting and/or a metasomatic enrichment episode(s) immediately prior to magma generation have to be invoked. The very pronounced subduction signature in the TAC supports the predominant melting of hydrated and HFSE-depleted lithospheric mantle, with subordinate contributions from upwelling asthenospheric mantle (Verdel et al., 2011). The occurrence of these alkaline rocks in a general setting of convergence is unusual, but can be attributed to periods of localized extension in the Lesser Caucasus. The overall convergence throughout Eocene and Oligocene is well

established based on kinematic data and modelling (Rosenbaum et al., 2002), but if the lithospheric structures allowed ascent of mantle-derived magmas via localized faulting and/or rift tectonics alkaline magmatism can develop even in collision zones (Harris et al., 1986). Development of an extensional regime along this sector of Lesser Caucasus was previously suggested to explain the alkaline character of Paleogene magmatic rocks, particularly those within Armenia (Kogarko et al., 1995).

7.4. Petrogenesis of pseudoleucite phonolites

Based on optical microscopy and geochemical analyses including XRD, 6 types of “epileucites” and 5 types of pseudoleucites were distinguished by their mineral associations, host rocks and crystallographic habit (Meliksetian, 1971, 1978). “Epileucites” are considered to be a result of post-magmatic hydrothermal alterations, whereas pseudoleucites are considered to be a result of disintegration of metastable K—Na leucite into mixture of orthoclase and nepheline under subsolidus conditions ($T = 600\text{ }^{\circ}\text{C}$) in late magmatic stage (Gittins et al., 1980; Meliksetian, 1978). Yagi and Gupta (1978) mention that the $\text{K}_2\text{O}/\text{Na}_2\text{O}$ ratio of 4.3 in pseudoleucites of porphyry tinguaita dykes of TAC is the highest among those studied worldwide highlighting the importance of resolving complex's evolutionary story to better understand the conditions of pseudoleucite paragenesis.

The investigated leucite pseudomorphs occur in a phonolite (Fig. 3c-f). Relicts of primary leucite are lacking, and they are generally rarely observed in leucite pseudomorphs. The leucite pseudomorphs mainly consist of alkali feldspar but do not contain nepheline, instead comprising abundant cancrinite (Fig. 13b–c). Different theories about the genesis of leucite pseudomorphs were put forward (see Edgar, 1984, and references therein), including (1) subsolidus breakdown of leucite to orthoclase and nepheline, (2) reaction of leucite with a Na-rich liquid and (3) alkali ion exchange reactions between leucites and Na-rich glass or fluid. We will briefly discuss these theories in relation to the leucite pseudomorphs in the phonolite.

Subsolidus breakdown of common K-rich leucite would produce alkali feldspar and kalsilite, hence a process to cause relative enrichment of Na is required to explain the occurrence of Na-bearing phases in pseudoleucites. Leucite solid solutions with up to 40 wt% $\text{NaAlSi}_2\text{O}_6$ were produced experimentally, and these experienced subsequent breakdown into nepheline and alkali feldspar (Fudali, 1963). However, natural leucite does not contain excess amount of sodium to form this type of intergrowth on decomposition (Viladkar, 2010). The mineralogy of the leucite pseudomorph, comprising abundant Na-bearing phases such as cancrinite and analcime (Fig. 13b–c), suggest that they are derived from a Na-rich precursor phase. Hence, subsolidus breakdown of natural K-rich leucite alone cannot explain their occurrence, but formation of a metastable Na-rich leucite before breakdown might be possible (Taylor & MacKenzie, 1975).

The pseudoleucite reaction is a reaction of leucite with a Na-rich magma to form alkali feldspar and nepheline in the system $\text{NaAlSiO}_4 - \text{KAlSiO}_4 - \text{SiO}_2$ (Bowen & Ellestad, 1937; Edgar, 1984). This reaction terminates the leucite stability field and leucite disappears by reaction with the magma (Bowen & Ellestad, 1937). The TAC leucite pseudomorphs, however, are characterized by a well-preserved deltoidal icositetrahedral crystal habit, reflecting the external shape of the precursor phase. It is difficult to envisage this reaction to fully replace primary leucite without modifying the morphology of the leucites (Taylor & MacKenzie, 1975), which is so beautifully preserved (Fig. 3). Moreover, various minor mineral phases that contain additional elements occur within the pseudomorphs. Some of these (e.g. clinopyroxene, apatite) may be explained as primary magmatic inclusions, but others (analcime, calcite) texturally appear as secondary phases (Fig. 13b–c). This suggests that explaining the genesis of the leucite pseudomorphs based on the phase relations in this petrogenetic system is an oversimplification (Edgar, 1984).

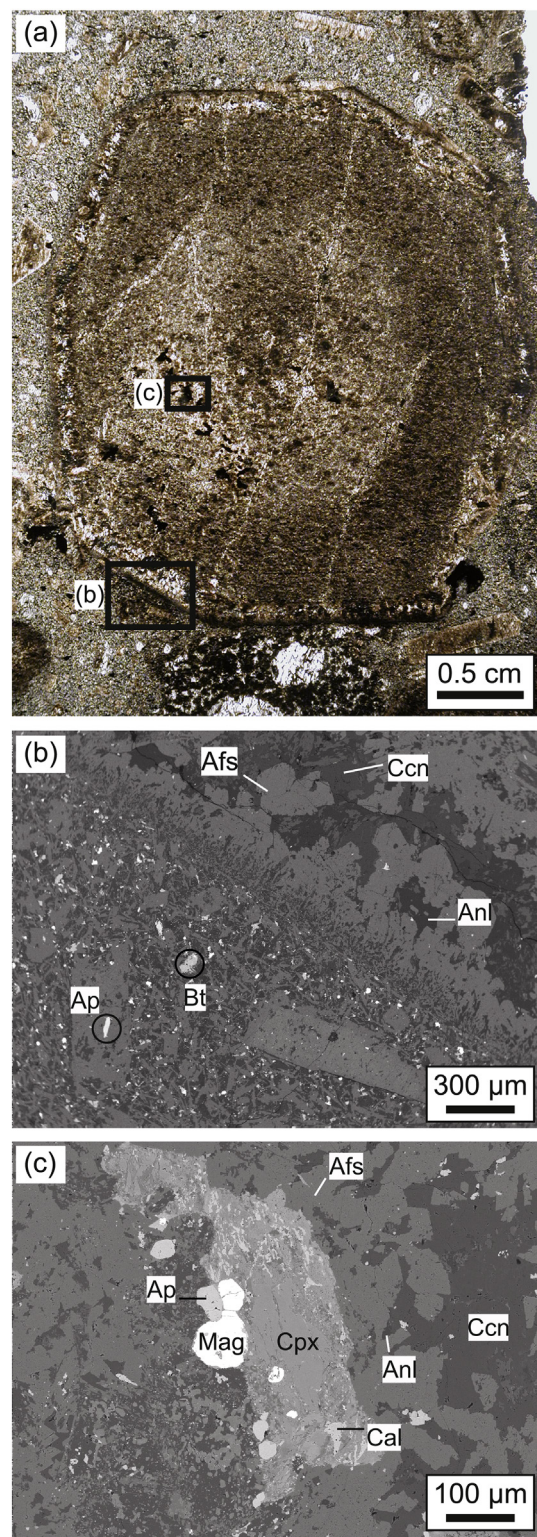


Fig. 13. Pseudoleucite from the OVV of the Tezhesar Complex. (a) Scanned thin section image of a single pseudoleucite crystal. (b,c) Back-scattered electron images of (b) the boundary between matrix and pseudoleucite and (c) the interior of the pseudoleucite. Note the presence of cancrinite (Ccn) and analcime (Anl), Cal = calcite, Mag = magnetite, other mineral abbreviations as in Fig. 4.

Alkali ion exchange reactions between leucites and Na-rich glass or fluid was proposed as mechanism to produce pseudomorphs after leucite that are similar in composition to natural pseudoleucites (Taylor & MacKenzie, 1975). Fluid-induced reactions would facilitate the increase in Na content and formation of Na-dominated phases, such as cancrinite

and analcime in TAC. Canocrinite is assumed to replace nepheline due to a reaction between nepheline and volatile-rich melts or fluids, a common late magmatic– hydrothermal process (Martins et al., 2017). A reaction with fluids was also used to explain pseudoleucite with intergrowth of alkali feldspar, sericite and canocrinite from the Gardar Province, Greenland (Hesselbo, 1986) and the replacement of nepheline by analcime, canocrinite, sodalite and muscovite in pseudoleucite from India (Viladkar, 2010). Canocrinite is also an important constituent of the pseudoleucite phenocrysts from Spotted Fawn Creek (Yukon Territory, Canada), where also garnet, biotite, calcite, muscovite and plagioclase occur as inclusions within pseudoleucite (Tempelman-Kluit, 1969). Removal of K, addition of Na and water was attributed to the entry of a fluid phase to permit the chemical exchange (Tempelman-Kluit, 1969). The presence of canocrinite in the TAC leucite pseudomorphs bears evidence for interaction with a H_2O - CO_2 -bearing fluid, possibly with minor amounts of S and Cl, as the general formula for canocrinite is $(Na,Ca,K)_{6-8}Al_{6-x}Si_{6+x}O_{24}(CO_3,SO_4,Cl,OH)_{1-2}\cdot nH_2O$ with $x < 1$ and $n = 1-5$ (Martins et al., 2017) illustrates. Given the scarcity of analcime in the TAC pseudoleucites, a conversion of primary leucites into analcime via reaction with Na-rich fluids as proposed for pseudoleucites from a phonolite dyke in Bohemia (Pivec et al., 2004) seems unlikely. The texture of the TAC leucite pseudomorphs pseudoleucites has resemblance to a “palisade texture”, in which orthoclase laths near the margins of the pseudomorphs are oriented at right angles to the crystal boundaries (Tempelman-Kluit, 1969). These textures can be interpreted to form by subsolidus reactions in response to increasing fluid pressure when pervasive fluids come in contact with the leucite (Hesselbo, 1986). All these lines of evidence point to a late/post-magmatic hydrothermal alteration for the formation of the leucite pseudomorphs in the investigated phonolite, and they can be referred to as “epileucites”. Complementary evidence for fluid-rich conditions during the late to post-magmatic evolution of the TAC are the presence of pegmatites and the widespread alteration in the CVU rocks.

8. Conclusions

- A combination of small degrees of partial melting and pre-conditioning of the mantle source by slab dehydration and subsequent metasomatic processes can explain the alkaline, subduction-influenced geochemical character of the TAC.
- The Sr—Nd isotopic data demonstrate a mantle source with negligible crustal influence. There is a broad isotopic overlap with Eocene to Quaternary magmatism in other regions of Armenia, suggesting the regional presence of isotopically similar mantle source regions.
- The emplacement of the syenitic units of the TAC was dated by $^{40}Ar/^{39}Ar$ at 41.0 ± 0.5 Ma. The emplacement of the TAC can thus be linked to a previously proposed model of Eocene Neotethyan slab rollback driving decompression melting and extension-related magmatism in Iran and Azerbaijan within a tectonic setting of general convergence between the Arabian and Eurasian plates.
- The formation of leucite pseudomorphs is related to initial leucite crystallization from an evolved, silica-undersaturated magma followed by subsolidus breakdown and interaction with a late to post-magmatic fluid. The magmatic-hydrothermal fluid percolating through the rocks caused alteration of nepheline into canocrinite and amphibolitisation of clinopyroxenes. This fluid overprint may be responsible for the plethora of REE-bearing phases described previously within the TAC and hence be a crucial factor in the (re)distribution of rare elements in alkaline igneous rocks.

Acknowledgements

This work is dedicated to the memory of Dr. Sci. Boris Meliksetian (1928–1992), who worked at the Institute of Geological Sciences of

the National Academy of Sciences of the Republic of Armenia and contributed a lot to our knowledge of Armenian magmatism through his studies of the petrology, mineralogy and geochemistry of igneous rocks in Armenia, the links of magmatism to geodynamics and ore-forming processes, and the Tezhsar alkaline ring complex in particular. We thank the Armenian National Academy of Sciences in Yerevan for logistical support during fieldwork. We also thank U. Westernströer for help with solution ICP-MS analyses in Kiel, A. Musiol for performing REE analyses in Potsdam, D. Wilde and P. Greatbatch for producing thin sections, and S. Whitley for advice on the discussion. V. Lebedev and an anonymous reviewer provided constructive comments that helped to improve the manuscript, and N. Eby is thanked for efficient editorial handling. Financial support through Santander Travel Bursaries to KS and RH for the 2015 field campaign is greatly appreciated.

Appendix A. Supplementary data

Supplementary data to this article can be found online at <https://doi.org/10.1016/j.lithos.2018.08.028>.

References

- Adamia, S., Zakariadze, G., Chkhouta, T., Sadradze, N., Tsreteli, N., Chabukiani, A., Gvengtsadze, A., 2011. *Geology of the Caucasus: a review*. Turkish Journal of Earth Sciences 20, 489–544.
- Agard, P., Omrani, L., Jolivet, L., Mouthereau, F., 2005. Convergence history across Zagros (Iran): constraints from collisional and earlier deformation. International Journal of Earth Sciences 94, 401–419.
- Agard, P., Omrani, L., Jolivet, L., Whitechurch, H., Vrielynck, B., Spakman, W., Monié, P., Meyer, B., Wortel, R., 2011. Zagros orogeny: a subduction-dominated process. Geological Magazine 148, 692–725.
- Aghamalyan, V.A., 1998. The crystalline basement of Armenia. Thesis of PhD dissertation. Institute of Geological Sciences of National Academy of Sciences, Yerevan, Armenia (in Russian).
- Allen, M.B., Armstrong, H.A., 2008. Arabia-Eurasia collision and the forcing of mid-Cenozoic global cooling. Palaeogeography, Palaeoclimatology, Palaeoecology 265, 52–58.
- Allen, M.B., Kheirkhah, M., Neill, I., Emami, M.H., McLeod, C.L., 2013. Generation of arc and within-plate chemical signatures in collision zone magmatism: quaternary lavas from Kurdistan Province, Iran. Journal of Petrology 54, 887–911.
- Arakelyan, R.A., 1964. The Paleozoic-Mesozoic. Geology of the Armenian SSR. Academy of Sciences of the Armenian SSR, Yerevan, pp. 21–163 (in Russian).
- Aslanyan, A.T., 1958. Regional Geology of Armenia. Haypetrap, Yerevan (in Russian).
- Aydinçakır, E., Şen, C., 2013. Petrogenesis of the post-collisional volcanic rocks from the Borcka (Artvin) area: implications for the evolution of the Eocene magmatism in the Eastern Pontides (NE Turkey). Lithos 172–173, 98–117.
- Bagdasaryan, G.P., 1966. Intrusive rocks of the Bazum-Pambak region. Geology of the Armenian SSR, Intrusive rocks. Academy of Sciences of the Armenian SSR, Yerevan, pp. 256–308 (in Russian).
- Bagdasaryan, G.P., Meliksetian, B.M., Ghukasyan, R.Kh., 1985. The alpine gneissic-granitic complex of the Zanguezor prominence pre-Alpine foundation. Earth Science letters. vol. 38(2). Academy of Sciences, Armenian SSR, Yerevan, pp. 9–20 (in Russian).
- Ballato, P., Uba, C.E., Landgraf, A., Strecker, M.R., Sudo, M., Stockli, D.F., Friedrich, A., Tabatabaei, S.H., 2011. Arabia-Eurasia continental collision: Insights from late Tertiary foreland-basin evolution in the Alborz Mountains, northern Iran. Geological Society of America Bulletin 123, 106–131.
- Belov, A.A., 1968. Boundary between Gondwana and Eurasia, and Palaeotethys suture in Caucasian sector of Mediterranean fold belt. Tectonics, structural geology, planetology. Works of Soviet geologists, XXV session of IGC, P83.
- Bodevign, S., Williams-Jones, A.E., Swinden, S., 2017. Carbonate-silicate melt immiscibility, REE mineralising fluids, and the evolution of the Lofdal Intrusive Suite, Namibia. Lithos 268, 383–398.
- Bonin, B., Azzouni-Sekkal, A., Bussy, F., Ferrag, S., 1998. Alkali-calcic and alkaline post-orogenic (PO) granite magmatism: petrologic constraints and geodynamic settings. Lithos 45, 45–70.
- Bowen, N.L., Ellestad, R.B., 1937. Leucite and pseudoleucite. American Mineralogist 22, 409–415.
- Boynton, W.V., 1984. Cosmochemistry of the rare earth elements; meteorite studies. In: Henderson, P. (Ed.), *Rare earth element geochemistry*. Elsevier, Amsterdam, pp. 63–114.
- Burke, K., Khan, S., 2006. Geoinformatic approach to global nepheline syenite and carbonatite distribution: testing a Wilson cycle model. Geosphere 2, 53–60.
- Chakhmouradian, A.R., Zaitsev, A.N., 2012. Rare earth mineralization in igneous rocks: sources and processes. Elements 8, 347–353.
- Connor, C., Connor, L., Halama, R., Meliksetian, K., Savov, I., 2011. *Volcanic Hazard Assessment of the Armenia Nuclear Power Plant Site Final Report Tampa*, Leeds, Yerevan.
- Costa, F., Andreastuti, S., Bouvet de Maisonneuve, C., Pallister, J.S., 2013. Petrological insights into the storage conditions, and magmatic processes that yielded the centennial 2010 Merapi explosive eruption. Journal of Volcanology and Geothermal Research 261, 209–235.

- Davidson, J., Turner, S., Handley, H., Macpherson, C., Dosseto, A., 2007. Amphibole "sponge" in arc crust? *Geology* 35, 787–790.
- Dawson, J.B., 1987. Metasomatised harzburgites in kimberlite and alkaline magmas; enriched restites and 'flushed' lherzolites. In: Menzies, M.A., Hawkesworth, C.J. (Eds.), *Mantle Metasomatism*. Academic Press, London, pp. 125–144.
- De La Roche, H., Leterrier, J., Grandclaude, P., Marchal, M., 1980. A classification of volcanic and plutonic rocks using R_1/R_2 -diagrams and major element analyses – its relationships with current nomenclature. *Chemical Geology* 29, 183–210.
- Delong, S.E., Hodges, F., Arculus, R.J., 1975. Ultramafic and mafic inclusions, Kanaga Island, Alaska and the occurrence of Alkaline Rocks in Island Arcs. *Journal of Geology* 83, 721–736.
- DePaolo, D.J., Wasserburg, G.J., 1979. Petrogenetic mixing models and Nd-Sr isotopic patterns. *Geochimica et Cosmochimica Acta* 43, 615–627.
- Dilek, Y., Imamverdiyev, N., Altunkaynak, S., 2010. Geochemistry and tectonics of Cenozoic volcanism in the Lesser Caucasus (Azerbaijan) and the peri-Arabian region: collision-induced mantle dynamics and its magmatic fingerprint. *International Geology Reviews* 52, 536–578.
- Downes, H., 1987. Tertiary and Quaternary volcanism in the Massif Central, France. In: Fitton, J.G., Upton, B.G.J. (Eds.), *Alkaline Igneous Rocks*. Geological Society Special Publications 30, pp. 517–530.
- Downes, H., Balaganskaya, E., Beard, A., Liferovich, R., Demaiffe, D., 2005. Petrogenetic processes in the ultramafic, alkaline and carbonatitic magmatism in the Kola Alkaline Province: a review. *Lithos* 85, 48–75.
- Dunworth, E.A., Bell, K., 2001. The Turyi massif, Kola peninsula, Russia: isotopic and geochemical evidence for a multi-source evolution. *Journal of Petrology* 42, 377–405.
- Edgar, A.D., 1984. Chemistry, occurrence and paragenesis of feldspathoids: a review. *NATO ASI Series, Series C: Mathematical and Physical Sciences* 137, 501–532.
- Eyboglu, Y.M., Santosh, M., Chung, S.-L., 2011. Crystal fractionation of adakitic magmas in the crust-mantle transition zone: Petrology, geochemistry and U-Pb zircon chronology of the Semer adakites, eastern Pontides, NE Turkey. *Lithos* 121, 151–166.
- Fitton, J.G., 1987. The Cameroon line, West Africa: a comparison between oceanic and continental alkaline volcanism. In: Fitton, J.G., Upton, B.G.J. (Eds.), *Alkaline Igneous Rocks*. Geological Society Special Publications 30, pp. 273–291.
- Fleck, R.J., Sutter, J.F., Elliot, D.H., 1977. Interpretation of discordant $^{40}\text{Ar}/^{39}\text{Ar}$ age-spectra of Mesozoic tholeiites from Antarctica. *Geochimica et Cosmochimica Acta* 41, 15–32.
- Frost, B.R., Frost, C.D., 2008. A geochemical classification for feldspathic igneous rocks. *Journal of Petrology* 49, 1955–1969.
- Frost, B.R., Arculus, R.J., Barnes, C.G., Collins, W.J., Ellis, D.J., Frost, C.D., 2001. A geochemical classification of granitic rocks. *Journal of Petrology* 42, 2033–2048.
- Fudali, R.F., 1963. Experimental studies bearing on the origin of pseudoleucite and associated problems of alkali rock systems. *Geological Society of America Bulletin* 74, 1101–1126.
- Ghukasyan, R.Kh., Tayan, R.N., Haruntunyan, M.A., 2006. Rb-Sr investigations of magmatic rocks of Kadjaran ore field (Republic of Armenia). Isotope Dating of Processes of Ore Mineralization, Magmatism, Sedimentation and Metamorphism, Materials of III Russian Conference on Isotope Geochronology I, pp. 213–216.
- Gittins, J., Fawcett, J.J., Brooks, C.K., Rucklidge, J.C., 1980. Intergrowths of nepheline-potassium feldspar and kalsilite-potassium feldspar: a re-examination of the 'pseudo-leucite problem'. *Contributions to Mineralogy and Petrology* 73, 119–126.
- Halama, R., Savov, I.P., Garbe-Schönberg, D., Schenk, V., Toulkeridis, T., 2013. Vesuvianite in high-pressure-metamorphosed oceanic lithosphere (Raspas complex, Ecuador) and its role for transport of water and trace elements in subduction zones. *European Journal of Mineralogy* 25, 193–219.
- Halama, R., Vennemann, T., Siebel, W., Markl, G., 2005. The Grønnedal-Ika carbonatite-syenite complex, South Greenland: Carbonatite formation by liquid immiscibility. *Journal of Petrology* 46, 191–217.
- Harris, N.B.W., Pearce, J.A., Tindle, A.G., 1986. Geochemical characteristics of collision-zone magmatism. *Geological Society of London Special Publications* 19, 67–81.
- Hässig, M., Rolland, Y., Sosson, M., Galoyan, G., Müller, C., Avagyan, A., Sahakyan, L., 2013. New structural and petrological data on the Amasia ophiolites (NW Sevan-Akera suture zone, Lesser Caucasus): insights for a large-scale obduction in Armenia and NE Turkey. *Tectonophysics* 588, 135–153.
- Hesselbo, S.P., 1986. Pseudoleucite from the Gardar of South Greenland. *Bulletin of Geological Society of Denmark* 35, 11–17.
- Hou, Z., Tian, S., Yuan, Z., Xie, Y., Yin, S., Yi, L., Yang, Z., 2006. The Himalayan collision zone carbonatites in western Sichuan, SW China: petrogenesis, mantle source and tectonic implication. *Earth and Planetary Science Letters* 244, 234–250.
- Innocenti, F., Mazzuoli, R., Pasquare, G., Radicati Di Brozolo, F., Villari, F., 1982. Tertiary and Quaternary volcanism of the Erzurum-Kars area (Eastern Turkey): geochronological data and geodynamic evolution. *Journal of Volcanology and Geothermal Research* 13, 223–240.
- Irvine, T.N., Baragar, W.R.A., 1971. A guide to the chemical classification of the common volcanic rocks. *Canadian Journal of Earth Sciences* 8, 523–548.
- Jackson, J., Haines, J., Holt, W., 1995. The accommodation of Arabia-Eurasia Plate convergence in Iran. *Journal of Geophysical Research* 100 (B8), 15205–15219.
- Jahn, B.-M., Wu, F., Lo, C.-H., Tsai, C.-H., 1999. Crust-mantle interaction induced by deep subduction of the continental crust: geochemical and Sr-Nd isotopic evidence from post-collisional mafic-ultramafic intrusions of the northern Dabie complex, Central China. *Chemical Geology* 157, 119–146.
- Johnson, S.E., Paterson, S.R., Tate, M.C., 1999. Structure and emplacement history of a multiple-center, cone-sheet bearing ring complex: the Zarza Intrusive complex, Baja California, Mexico. *Geological Society of America Bulletin* 111, 607–619.
- Jung, S., Hoffer, E., Hoernes, S., 2007. Neo-Proterozoic rift-related syenites (Northern Damara Belt, Namibia): Geochemical and Nd-Sr-Pb-O isotope constraints for mantle sources and petrogenesis. *Lithos* 96, 415–431.
- Kaislaniemi, L., van Hunen, J., Allen, M.B., Neill, I., 2014. Sublithospheric small-scale convection – a mechanism for collision zone magmatism. *Geology* 42, 291–294.
- Karakhanian, A., Jrashian, R., Trifonov, V., Philip, H., Arakelian, S., Avagian, A., 2002. Holocene-historical volcanism and active faults as natural risk factors for Armenia and adjacent countries. *Journal of Volcanology and Geothermal Research* 113, 319–344.
- Karapetian, S., Jrashian, R., Mnatsakanian, A., 2001. Late collision rhyolitic volcanism in the north-eastern part of the Armenian highland. *Journal of Volcanology and Geothermal Research* 112, 189–220.
- Kazemi, K., Kananian, A., Xia, Y., Sarjoughian, F., 2018. Petrogenesis of Middle-Eocene granitoids and their Mafic microgranular enclaves in central Urmia-Dokhtar Magmatic Arc (Iran): evidence for interaction between felsic and mafic magmas. *Geoscience Frontiers* <https://doi.org/10.1016/j.gsf.2018.04.006>.
- Kepezhinskis McDermott, P., 1997. Trace element and Sr-Nd-Pb isotopic constraints on a three-component model of Kamchatka arc petrogenesis. *Geochimica et Cosmochimica Acta* 61:577–600. [https://doi.org/10.1016/S0016-7037\(96\)00349-3](https://doi.org/10.1016/S0016-7037(96)00349-3).
- Keskin, M., Pearce, J.A., Mitchell, J.G., 1998. Volcano-stratigraphy and geochemistry of collision-related volcanism on the Erzurum-Kars Plateau, northeastern Turkey. *Journal of Volcanology and Geothermal Research* 85, 355–404.
- Keskin, M., 2003. Magma generation by slab steepening and breakoff beneath a subduction-accretion complex: an alternative model for collision-related volcanism in Eastern Anatolia, Turkey. *Geophysical Research Letters* 30 (24):1–4. <https://doi.org/10.1029/2003GL018019>.
- Kheirkhah, M., Allen, M.B., Emami, M., 2009. Quaternary syn-collision magmatism from the Iran/Turkey borderlands. *Journal of Volcanology and Geothermal Research* 182, 1–12.
- Kheirkhah, M., Neill, I., Allen, M.B., 2015. Petrogenesis of OIB-like basaltic volcanic rocks in a continental collision zone: late Cenozoic magmatism of Eastern Iran. *Journal of Asian Earth Sciences* 106, 19–33.
- Knipper, A.L., Khain, E.V., 1980. Structural position of ophiolites of the Caucasus. *Ophioliti* 2, 297–314.
- Kogarko, L.N., Konova, V.A., Orlova, M.P., Woolley, A.R., 1995. Caucasus (Armenia, Azerbaijan, Georgia). In: Kogarko, L. (Ed.), *Alkaline Rocks and Carbonatites of the World, Part Two: Former USSR*. Springer, Dordrecht, pp. 59–64.
- Kotlyar, V.N., 1958. *Pambak*. Academy of Sciences, Armenian SSR, Yerevan (in Russian).
- Kramm, U., Kogarko, L.N., 1994. Nd and Sr isotope signatures of the Khibina and Lovozero agpaitic centres, Kola Province, Russia. *Lithos* 32, 225–242.
- La Flèche, M.R., Camiré, G., Jenner, G.A., 1998. Geochemistry of post-Acadian, Carboniferous continental intraplate basalts from the Maritimes Basin, Magdalen Islands, Québec, Canada. *Chemical Geology* 148, 115–136.
- Lan, T.-G., Fan, H.-R., Hu, F.-F., Tomkins, A.G., Yang, K.-F., Liu, Y., 2011. Multiple crust-mantle interactions for the destruction of the North China Craton: geochemical and Sr-Nd-Pb-Hf isotopic evidence from the Longbaoshan alkaline complex. *Lithos* 122, 87–106.
- Lebedev, V.A., Bubnov, S.N., Chernyshev, I.V., Chugaev, A.V., Dudauri, O.Z., Vashakidze, G.T., 2007. *Geochronology and genesis of subalkaline basaltic lava rivers at the Dzhavakheti Highland, Lesser Caucasus: K-Ar and Sr-Nd isotopic data*. *Geochemistry International* 45, 211–225.
- Lebedev, V.A., Chernyshev, I.V., Shatagin, K.N., Bubnov, S.N., Yakushev, A.I., 2013. The quaternary volcanic rocks of the Geghama Highland, Lesser Caucasus, Armenia: geochronology, isotopic Sr-Nd characteristics, and origin. *Journal of Volcanology and Seismology* 7, 204–229.
- Lebedev, V.A., Sakhno, V.G., Yakushev, A.I., 2009. Late Cenozoic volcanic activity in Western Georgia: evidence from new isotope geochronological data. *Doklady Earth Sciences* 427, 819–825.
- Lordkipanidze, M.B., Meliksetian, B.M., Jrashian, R., 1989. Mesozoic-Cenozoic magmatic evolution of the Pontian-Crimean-Caucasian region. In: Rakuš, M., Dercourt, J., Laird, A.E.M. (Eds.), *Evolution of the Northern Margin of Tethys, ICP Project 198. Mémoire Société Géologique France*, Paris, Nouvelle Série 154, pp. 103–124.
- Magakyan, I. (Ed.), 1981. Magmatic and metamorphic formations of the Armenian SSR. *Akademija Nauk Armyanskoi SSR*, Yerevan.
- Mamani, M., Wörner, G., Sempere, T., 2010. Geochemical variations in igneous rocks of the central Andean orocline ($13^{\circ}S$ – $18^{\circ}S$): Tracing crustal thickening and magma generation through time and space. *Geological Society of America Bulletin* 122, 162–182.
- Marks, M.A.W., Vennemann, T., Siebel, W., Markl, G., 2004. Nd-, O-, H-isotopic evidence for complex, closed-system fluid evolution of the peralkaline Ilímaussaq intrusion, South Greenland. *Geochimica et Cosmochimica Acta* 68, 3379–3395.
- Marks, M.A.W., Schilling, J., Coulson, I.M., Wenzel, T., Markl, G., 2008. The Alkaline-Peralkaline Tazmazeght complex, High Atlas Mountains, Morocco: Mineral Chemistry and Petrological Constraints for Derivation from a Compositionally Heterogeneous Mantle Source. *Journal of Petrology* 49, 1097–1131.
- Martins, T., Kressall, R., Medici, L., Chakhmouradian, A.R., 2017. Cancrinite-vishnevite solid solution from Cinder Lake (Manitoba, Canada): crystal chemistry and implications for alkaline igneous rocks. *Mineralogical Magazine* 81:1261–1277. <https://doi.org/10.1180/minmag.2016.080.165>.
- Mazhari, S.A., Bea, F., Amini, S., Ghahamghash, J., Molina, J.F., Montero, P., Scarrow, J.H., Williams, I.S., 2009. The Eocene bimodal Piranshahr massif of the Sanandaj-Sirjan Zone, NW Iran: a marker of the end of the collision in the Zagros orogeny. *Journal of the Geological Society of London* 166, 53–69.
- McDonough, W.F., Sun, S.-S., 1995. Composition of the Earth. *Chemical Geology* 120: 223–253. [https://doi.org/10.1016/0009-2541\(94\)00140-4](https://doi.org/10.1016/0009-2541(94)00140-4).
- Mederer, J., Moritz, R., Ulianov, A., Chiaradia, M., 2013. Middle Jurassic to Cenozoic evolution of arc magmatism during Neotethys subduction and arc-continent collision in the Kapan Zone, southern Armenia. *Lithos* 177, 61–78.
- Meliksetian, B.M., 1970. About the problem of genesis of pseudoleucite and leucite bearing rocks of Tezhsar Alkaline complex. *Earth Science Letters, Academy of Sciences, Armenian SSR, Yerevan* 3, 61–85 (in Russian).

- Meliksetian, B.M., 1971. Mineralogy, geochemistry and petrology of Tezhsar Alkaline Complex. Intrusive complexes of principal ore provinces of Armenia. Academy of Sciences, Armenian SSR, Yerevan, pp. 117–298 (in Russian).
- Meliksetian, B.M., 1978. Genesis of Pambak pseudoleucites (Armenia). XI General Meeting of International Mineralogical Association, Novosibirsk, Abstracts. vol. 1, pp. 36–37.
- Meliksetian, B.M., 1989. Petrology, Geochemistry and Ore Genesis of Palaeogene–Neogene Volcano-Intrusive Formations of Lesser Caucasus (Magmatism of Collision Zones). Thesis of Doc. Sci. dissertation. Academy of Science, Tbilisi, Georgian SSR (in Russian).
- Melkonyan, R.L., Ghkasiyan, R.K.H., Tayan, R.N., Haruntunyan, M.A., 2008. Geochronometry of the Meghri pluton monzonites (Armenia) – results and consequences. Proceedings of the National Academy of Sciences of the Republic of Armenia 61, 3–9 (in Russian with English abstract).
- Moritz, R., Rezeau, H., Ovtcharova, M., Tayan, R., Melkonyan, R., Hovakimyan, S., Ramazanov, V., Selby, D., Ulianov, A., Chiaradia, M., Putlitz, B., 2016. Long-lived, stationary magmatism and pulsed porphyry systems during Tethyan subduction to post-collision evolution in the southernmost Lesser Caucasus, Armenia and Nakhichevan. *Gondwana Research* 37, 465–503.
- Neill, I., Meliksetian, Kh., Allen, M.B., Navasardyan, G., Karapetyan, S., 2013. Pliocene–Quaternary volcanic rocks of NW Armenia: magmatism and lithospheric dynamics within an active orogenic plateau. *Lithos* 180–181, 200–215.
- Neill, I., Meliksetian, Kh., Allen, M.B., Navasardyan, G., Kuiper, K., 2015. Petrogenesis of mafic collision zone magmatism: the Armenian sector of the Turkish–Iranian Plateau. *Chemical Geology* 403, 24–41.
- Pearce, J.A., Bender, J.F., Delong, S.E., Kidd, W.S.F., Low, P.J., Guner, Y., Sargol, F., Yilmaz, Y., Moorbath, S., Mitchell, J.C., 1990. (Genesis of collision volcanism in eastern Anatolia), Turkey. *Journal of Volcanology and Geothermal Research* 44, 189–229.
- Phillip, H., Cicternas, A., Gvishiani, A., Gorshkov, A., 1989. The Caucasus: an actual example of the initial stages of continental collision. *Tectonophysics* 161, 1–21.
- Pivec, E., Ulrych, J., Langrová, A., 2004. On the origin of pseudoleucite from Cenozoic phonolite dyke from Loučná/Böhmisch Wiesenthal, Krušné hory/Erzgebirge Mts., Bohemia. *Neues Jahrbuch für Mineralogie – Abhandlungen* 179, 221–238.
- Rezeau, H., Moritz, R., Leuthold, J., Hovakimyan, S., Tayan, R., Chiaradia, M., 2017. 30 Myr of Cenozoic magmatism along the Tethyan margin during Arabia–Eurasia accretionary orogenesis (Meghri–Ordubad pluton, southernmost Lesser Caucasus). *Lithos* 288–289, 108–124.
- Rolland, Y., 2017. Caucasus collisional history: Review of data from East Anatolia to West Iran. *Gondwana Research* 49, 130–146.
- Rolland, Y., Billot, S., Corsini, M., Sosson, M., Galoyan, G., 2009a. Blueschists of the Amassia–Stepanavank Suture Zone (Armenia): linking Tethys subduction history from E-Turkey to W-Iran. *International Journal of Earth Sciences* 98, 533–550.
- Rolland, Y., Galoyan, G., Bosch, D., Sosson, M., Corsini, M., Fornari, M., Verati, C., 2009b. Jurassic back-arc and Cretaceous hot-spot series in the Armenian ophiolites – implications for the obduction process. *Lithos* 112, 163–187.
- Rosenbaum, G., Lister, G.S., Duboz, C., 2002. Relative motions of Africa, Iberia and Europe during Alpine orogeny. *Tectonophysics* 359, 117–129.
- Sahakyan, L., Bosch, D., Sosson, M., Avagyan, A., Galoyan, Gh., Rolland, Y., Bruguier, O., Stepanyan, Zh., Galland, B., Vardanyan, S., 2016. Geochemistry of the Eocene magmatic rocks from the Lesser Caucasus area (Armenia): evidence of a subduction geodynamic environment. *Geological Society of London Special Publications* 428, 73.
- Schiano, P., Monzier, M., Eissen, J.-P., Martin, H., Koga, K.T., 2010. Simple mixing as the major control of the evolution of volcanic suites in the Ecuadorian Andes. *Contributions to Mineralogy and Petrology* 160, 297–310.
- Sheth, H., Meliksetian, Kh., Gevorgyan, H., Israyelyan, A., Navasardyan, G., 2015. Intracanyon basalt lavas of the Debed River (northern Armenia), part of a Pliocene–Pleistocene continental flood basalt province in the South Caucasus. *Journal of Volcanology and Geothermal Research* 295, 1–15.
- Shand, S.J., 1947. *The Eruptive Rocks*. 3rd Ed. Wiley, New York.
- Sindern, S., Kramm, U., 2000. Volume characteristics and element transfer of fenite aureoles: a case study from the Iivaara alkaline complex, Finland. *Lithos* 51, 75–93.
- Smith, I.E.M., White, A.J.R., Chappell, B.W., Eggleton, R.A., 1988. Fractionation in a zoned monzonite pluton: Mount Dromedary, southeastern Australia. *Geological Magazine* 125, 273–284.
- Sosson, M., Rolland, Y., Müller, C., Danelian, T., Melkonyan, R., Kekelia, S., Adamia, S., Babazadeh, V., Kangarli, T., Avagyan, A., Galoyan, G., Mosar, J., 2010. Subductions, obduction and collision in the Lesser Caucasus (Armenia, Azerbaijan, Georgia), new insights. *Geological Society Special Publications* 340, 329–352.
- Suikkanen, E., Rämö, O.T., 2017. Metasomatic alkali-feldspar syenites (episyenites) of the Proterozoic Suomenniemi rapakivi granite complex, southeastern Finland. *Lithos* 294–295, 1–19.
- Taylor, D., MacKenzie, W.S., 1975. A contribution to the pseudoleucite problem. *Contributions to Mineralogy and Petrology* 49, 321–333.
- Tempelman-Kluit, D.J., 1969. A re-examination of pseudoleucite from Spotted Fawn Creek, west-central Yukon. *Canadian Journal of Earth Sciences* 6, 55–62.
- Trumbull, R.B., Bühn, B., Romer, R.L., Volker, F., 2003. The petrology of basanite-tephrite intrusions in the Erongo complex and implications for a plume origin of Cretaceous alkaline complexes in Namibia. *Journal of Petrology* 44, 93–112.
- Upton, B.G.J., Emeleus, C.H., Heaman, L.M., Goodenough, K.M., Finch, A.A., 2003. Magmatism of the mid-Proterozoic Gardar Province, South Greenland: chronology, petrogenesis and geological setting. *Lithos* 68, 43–65.
- Uto, K., Ishizuka, O., Matsumoto, A., Kamioka, H., Togashi, S., 1997. Laser-heating $^{40}\text{Ar}/^{39}\text{Ar}$ dating system of the Geological Survey of Japan: system outline and preliminary results. *Bulletin of Geological Survey of Japan* 48, 23–46.
- Van Hunen, J., Allen, M.B., 2011. Continental collision and slab break-off: a comparison of 3-D numerical models with observations. *Earth and Planetary Science Letters* 302, 27–37.
- Verdel, C., Wernicke, B.P., Hassanzadeh, J., Guest, B., 2011. A Paleogene extensional arc flare-up in Iran. *Tectonics* 30. <https://doi.org/10.1029/2010TC002809> TC3008.
- Viladkar, S.G., 2010. The origin of pseudoleucite in tinguaita, Ghori, India: a re-evaluation. *Petrology* 18, 544–554.
- Vincent, S.J., Allen, M.B., Ismail-Zadeh, A.D., Flecker, R., Foland, K.A., Simmons, M.D., 2005. Insights from the Talysh of Azerbaijan into the Paleogene evolution of the South Caspian region. *Geological Society of America Bulletin* 117, 1513–1533.
- Williams, H.M., Turner, S.P., Pearce, J.A., Kelley, S.P., Harris, N.B.W., 2004. Nature of the source regions for post-collisional potassic magmatism in southern and northern Tibet from geochemical variations and inverse trace element modelling. *Journal of Petrology* 45, 555–607.
- Woodhead, J.D., Hergt, J.M., Davidson, J.P., Egging, S.M., 2001. Hafnium isotope evidence for ‘conservative’ element mobility during subduction zone processes. *Earth and Planetary Science Letters* 192, 331–346.
- Woolley, A.R., 2001. *Alkaline Rocks and Carbonatites of the World, Part 3: Africa*. The Geological Society, London.
- Yagi, K., Gupta, A.K., 1978. Pseudoleucite from Tezharsk, USSR, and its genesis. XI General Meeting of International Mineralogical Association, Novosibirsk, Abstracts. vol. 1, pp. 38–39.
- Zavarický, A., 1934. About pseudoleucite and epieleucite rocks. *Reports of the Academy of Sciences SSSR* N8–9.
- Zhang, K.-J., Li, Q.-H., Yan, L.-L., Zeng, L., Lu, L., Zhang, Y.-X., Hui, J., Jin, X., Tang, X.-C., 2017. Geochemistry of limestones deposited in various plate tectonic settings. *Earth-Science Reviews* 167, 27–64.
- Zhao, Z.-F., Dai, L.-Q., Zheng, J.-F., 2013. Post-collisional mafic igneous rocks record crust–mantle interaction during continental deep subduction. *Nature Scientific Reports* 3, 3413.